

# Text and Figures for ScholarWorks@UA collection

Seismic moment tensor results for nine events in the North Korea region

Celso Alvizuri

Version 1: May 25, 2018

Version 2: August 8, 2018

**Attribution:** If you use these files, please cite *Alvizuri and Tape* (2018) and *Alvizuri* (2018). This document is downloadable as a pdf via the link listed in *Alvizuri* (2018).

## Description of files

A summary of files in the collection is listed in the following table:

file name	description
scholarworks_nkfmtu.pdf	this file: summary of collection, including waveform fits and uncertainty figures
nkfmtu_mech_4sta_extended.txt	text file catalog of moment tensors; inversions using 4 stations
nkfmtu_mech_allsta_extended.txt	text file catalog of moment tensors; inversions using all stations
nkfmtu_allsta_explosion_K1_mech_extended.txt nkfmtu_allsta_explosion_D1_mech_extended.txt	text file catalogs of six explosions decomposed into the first crack-plus-double-couple ( <i>Alvizuri and Tape</i> , 2018, Figure 7): $M = K_1 + D_1$
nkfmtu_allsta_explosion_K2_mech_extended.txt nkfmtu_allsta_explosion_D2_mech_extended.txt	text file catalogs of six explosions decomposed into the second crack-plus-double-couple ( <i>Alvizuri and Tape</i> , 2018, Figure 7): $M = K_2 + D_2$
nkfmtu_weights_4sta.zip	zipped set of text files of input parameters for moment tensor inversions with 4 stations
nkfmtu_weights.zip	zipped set of text files of input parameters for moment tensor inversions with all stations

## Waveform fits: Figures D1–D9

Waveform fits for nine moment tensor inversions for which waveform misfit is plotted on the source-type plot. Black are observed waveforms; red are synthetic waveforms computed using a frequency-wavenumber method (*Zhu and Rivera*, 2002) that assumes a (1D) layered model. The waveforms are fit separately within five time windows: P wave vertical component (PV), P wave radial component (PR), Rayleigh wave vertical component (SurfV), Rayleigh wave horizontal component (SurfR), and Love wave transverse component (SurfT). At far left in each row is the station name, source-station distance in km, and station azimuth in degrees. Below each pair of waveforms are four numbers: the cross-correlation time shift between data and synthetics, the

cross-correlation value, the percent of the misfit function represented by the waveform pair, and the amplitude ratio between waveforms,  $\ln(A_{\text{obs}}/A_{\text{syn}})$ , where  $A$  is the max value of the waveform within the time window.

The beachball represents the best solution  $M_0$  (i.e., the global minimum of the misfit function). The beachball is plotted as a lower-hemisphere projection (standard seismological convention) of the moment tensor. The surrounding black dots denote the azimuthal location of the stations used, and the red crosses denote the lower hemisphere piercing points of the ray paths to the stations.

Here is a header for an example event in Figure D1:

```
Event 20061009013528000 Model MDJ2 Depth 1
FM 22 86 85 Mw 3.84 γ -18 δ 53 rms 3.931e-01 VR 84.5 pol_wt 999.00
Filter periods (seconds): Body:0.10-10.00. Surf:16.67-33.33 duration: 1.00/0.50 s
# norm L1 # Pwin 1 Swin 400 # N 18 Np 0 Ns 24
```

The four header lines are as follows:

1. Event 20061009013528000 Model MDJ2 Depth 1

The event ID is derived from the origin time of 2006-10-09 01:35:28.000

The layered model used is MDJ2, and the event depth is 1 km.

2. FM 22 86 85 Mw 3.84 γ -18 δ 53 rms 3.931e-01 VR 84.5 pol\_wt 999.00

The orientation of the moment tensor solution  $M_0$  is strike  $22^\circ$ , dip  $86^\circ$ , rake  $85^\circ$ . The estimated magnitude is  $M_w 3.84$ . The source type of  $M_0$  is expressed in terms of lune longitude  $\gamma = -18^\circ$  and lune latitude  $\delta = 53^\circ$ . The waveform difference between data and synthetics is  $RMS = 0.3931$ , and the variance reduction is  $VR = 84.5\%$ . These are based on a waveform difference measure that rewards using longer time windows and broader bandpass limits. This choice means that the  $VR$  cannot be directly compared with  $VR$  values reported in other studies.

If polarities are used in the misfit function, then the factor `pol_wt` determines the balance between fitting waveforms and fitting polarities. A value of 999.0 means that polarities are not used.

3. Filter periods (seconds): Body:0.10-10. Surf:6.67-33.33 duration: 1.00/0.50 s

The body waves, if used in the inversions, were filtered 0.10–10 s, the surface waves were filtered 6.67–33.33 s.

The source time function is a trapezoidal function whose duration is 1.00 s and whose rise time is half the duration. The duration is not an estimated source parameter but is set according to the target frequency of body waveforms (here 1–10 Hz).

4. # norm L1 # Pwin 1 Swin 400 # N 18 Np 0 Ns 24

An L1 norm was used for the misfit function (e.g., *Silwal and Tape*, 2016). The (reference) P-window is 1 s long and the surface wave window is 400 s long. There are 18 stations (N), 0 P wave windows (Np), and 24 surface wave windows (Ns).

The numbers below each station are

1. source-station epicentral distance, km

2. station azimuth, in degrees
3. time shift between picked P onset and synthetic P onset.
4. sign of the observed first-motion polarity<sup>1</sup>, which is either 1 (up or compression) or  $-1$  (down or dilatation). The number in parentheses is the predicted amplitude, which ranges between  $\pm\sqrt{2}$ ; numbers close to zero indicate that the station is near a nodal surface of the radiation pattern for the assumed mechanism.

The four numbers below each pair of waveforms are

1. the cross-correlation time shift  $\Delta T = T_{\text{obs}} - T_{\text{syn}}$  required for matching the synthetics  $s(t)$  with the data  $u(t)$ . A positive time-shift means that the synthetics arrive earlier than the data and that the assumed velocity model is faster than the actual earth structure.
2. the maximum cross-correlation percentage between  $u(t)$  and  $s(t - \Delta T)$
3. the percentage of the total misfit
4. the amplitude ratio  $\ln(A_{\text{obs}}/A_{\text{syn}})$  in each time window

## Uncertainty plots: Figures D10–D18

*Alvizuri and Tape* (2018), Figure 4, caption:

Full moment tensor uncertainty summary for the NK6 explosion event.

(a) Map of source location (red star) and stations used in the inversion for this event. The station is colored blue if the observed first-motion polarity on the vertical component is up (compression) and white if it is down (dilatation). (b) Contour plot of the polarity misfit on the lune. (c) Source type probability density  $p(v, w)$  in the  $vw$  rectangle (*Tape and Tape*, 2015). A green circle indicates the location of the point  $(v_x, w_x)$  where  $p$  is maximum; this point is apt to differ from the source type  $(v_0, w_0)$  of  $M_0$ . (d) Contour plot of the variance reduction  $VR(\Lambda)$ . At each point  $\Lambda$ , the variance reduction  $VR(\Lambda)$  is the maximum variance reduction  $VR(M)$  for moment tensors  $M$  that have source type  $\Lambda$ . Large values (blue) of  $VR$  represent better fit between observed and synthetic waveforms. Of the beachballs  $M(\Lambda)$ , our solution  $M_0$  (green box) is the one with largest  $VR$ . The gray arcs on the lune are the great circle arcs  $\lambda_1 = 0$ ,  $\lambda_2 = 0$ , and  $\lambda_3 = 0$ . Selected eigenvalue triples (black dots) on the boundary of the lune are indicated, with the understanding that the triples need to be normalized. The positive isotropic source  $(1, 1, 1)$  is at the top, the negative isotropic source  $(-1, -1, -1)$  is at the bottom, and the double couple  $(1, 0, -1)$ , not shown, would be at the center of the lune. (e) The curves  $\hat{V}'(\omega)$  and  $\hat{P}'(\omega)$  that are used to construct the confidence curve  $\mathcal{P}(V)$  in (f), as explained in *Silwal and Tape* (2016) in the context of double couples. For full moment tensors, as here,  $\hat{V}'(\omega) \propto \sin^4 \omega$ . (f) The confidence curve  $\mathcal{P}(V)$  for  $M_0$ . The more the curve resembles the shape of a capital gamma ( $\Gamma$ ), the better. The shaded area is the average confidence  $\mathcal{P}_{\text{AV}}$ . (g) The moment tensor  $M_0$ , plotted in a lower-hemisphere projection. The location of the piercing point for each station depends on the station azimuth, epicentral distance, and the assumed layered reference model.

---

<sup>1</sup>First-motion polarity measurements were only used for the NK6 event (*Alvizuri and Tape*, 2018).

## Time shift maps per event: Figures D19–D20

For each event, we can collect the time shifts for Rayleigh waves and Love waves and plot them as “spider” plots. These plots are useful in assessing the possibility of cycle skipping between observed and synthetic waveforms. Since the time shifts are expected to be caused by differences between real Earth structure and the assumed 1D Earth structure, we expect the time shift patterns to be smoothly varying as the station azimuth changes. However, the time shifts can also be caused by errors in the assumed source hypocenter or origin time; hence we also examine the time shift plots per station.

## Lune figures comparing the number of stations: Figures D21–D29

For each event, we compare moment tensor uncertainties using four stations and all stations. These comparisons are useful to see the impact of the number of stations on the uncertainty estimates.

## Text file tables for moment tensor catalogs [nkfmtu\_mech\_XXXX\_extended.txt]

Seismic moment tensor catalogs. Details can be found within the header lines, which also refer to *Kanamori* (1977); *Aki and Richards* (1980); *Silver and Jordan* (1982); *Minson et al.* (2007); *Tape and Tape* (2012, 2013, 2015).

## Input text files used in the moment tensor inversion [nkfmtu\_weights\_XXXX.zip]

We provide a text file for each of the nine events in this study. These files show which stations and which time windows were used (or not) in each moment tensor inversion. It also shows the first-motion polarity observations that were used.

## References

- Aki, K., and P. G. Richards (1980), *Quantitative Seismology, Theory and Methods*, W. H. Freeman, San Francisco, Calif., USA.
- Alvizuri, C. (2018), Seismic moment tensor results for nine events in the North Korea region, ScholarWorks@UA at <http://hdl.handle.net/11122/8441>: descriptor file with figures, text files of catalog, and input weight files.
- Alvizuri, C., and C. Tape (2018), Full moment tensor analysis of nuclear explosions in North Korea, *Seismol. Res. Lett.* (in press).
- Kanamori, H. (1977), The energy release in great earthquakes, *J. Geophys. Res.*, *82*, 2981–2987.
- Minson, S. E., D. S. Dreger, R. Bürgmann, H. Kanamori, and K. M. Larson (2007), Seismically and geodetically determined nondouble-couple source mechanisms from the 2000 Miyakejima volcanic earthquake swarm, *J. Geophys. Res.*, *112*, B10308, doi:10.1029/2006JB004847.
- Silver, P. G., and T. H. Jordan (1982), Optimal estimation of scalar seismic moment, *Geophys. J. R. Astron. Soc.*, *70*, 755–787.
- Silwal, V., and C. Tape (2016), Seismic moment tensors and estimated uncertainties in southern Alaska, *J. Geophys. Res. Solid Earth*, *121*, 2772–2797, doi:10.1002/2015JB012588.
- Tape, W., and C. Tape (2012), A geometric setting for moment tensors, *Geophys. J. Int.*, *190*, 476–498, doi:10.1111/j.1365-246X.2012.05491.x.
- Tape, W., and C. Tape (2013), The classical model for moment tensors, *Geophys. J. Int.*, *195*, 1701–1720, doi:10.1093/gji/ggt302.
- Tape, W., and C. Tape (2015), A uniform parameterization of moment tensors, *Geophys. J. Int.*, *202*, 2074–2081, doi:10.1093/gji/ggv262.
- Zhu, L., and L. A. Rivera (2002), A note on the dynamic and static displacements from a point source in multilayered media, *Geophys. J. Int.*, *148*, 619–627, doi:10.1046/j.1365-246X.2002.01610.x.

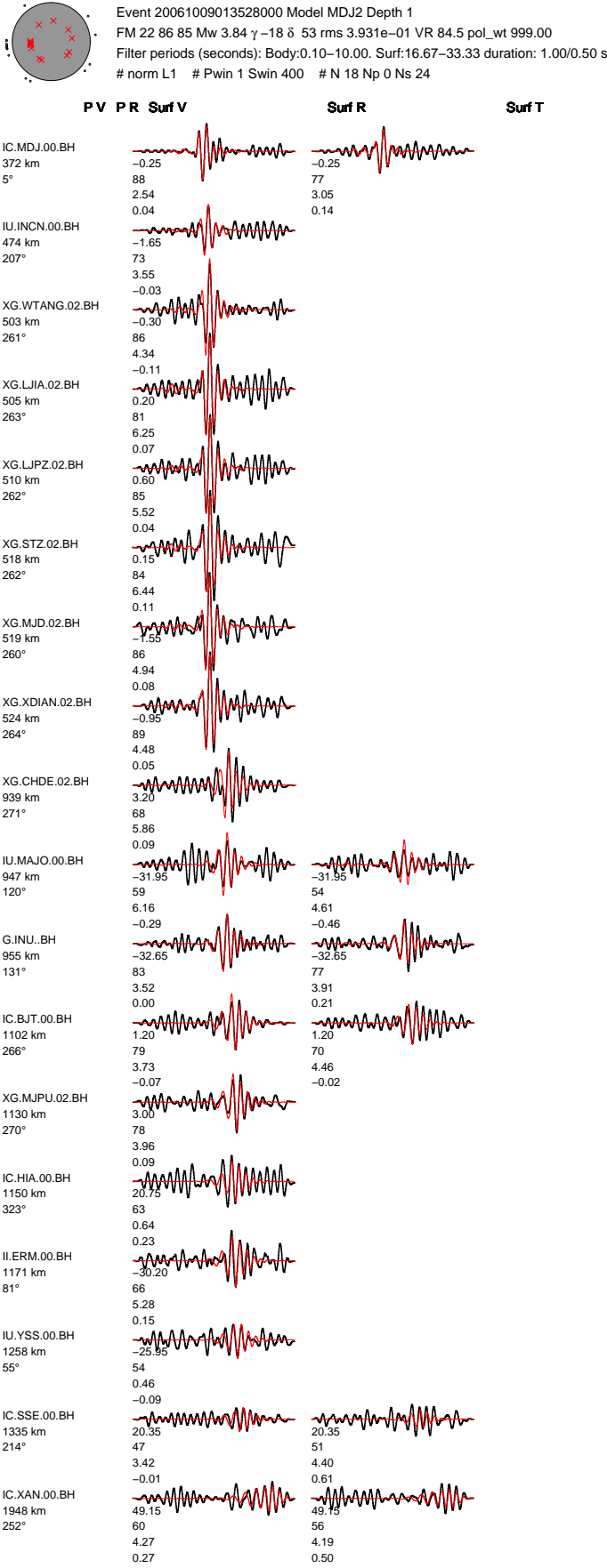


Figure D1: Best-fitting moment tensor and waveform fits for event NK1. Red = time-shifted synthetics, black = data. For each station, the three time windows are for Rayleigh waves (Surf V, Surf R) and for Love waves (Surf T). Numbers beneath each waveform pair are the time shift, the cross correlation maximum, the percentage of the misfit function, and the log amplitude ratio.

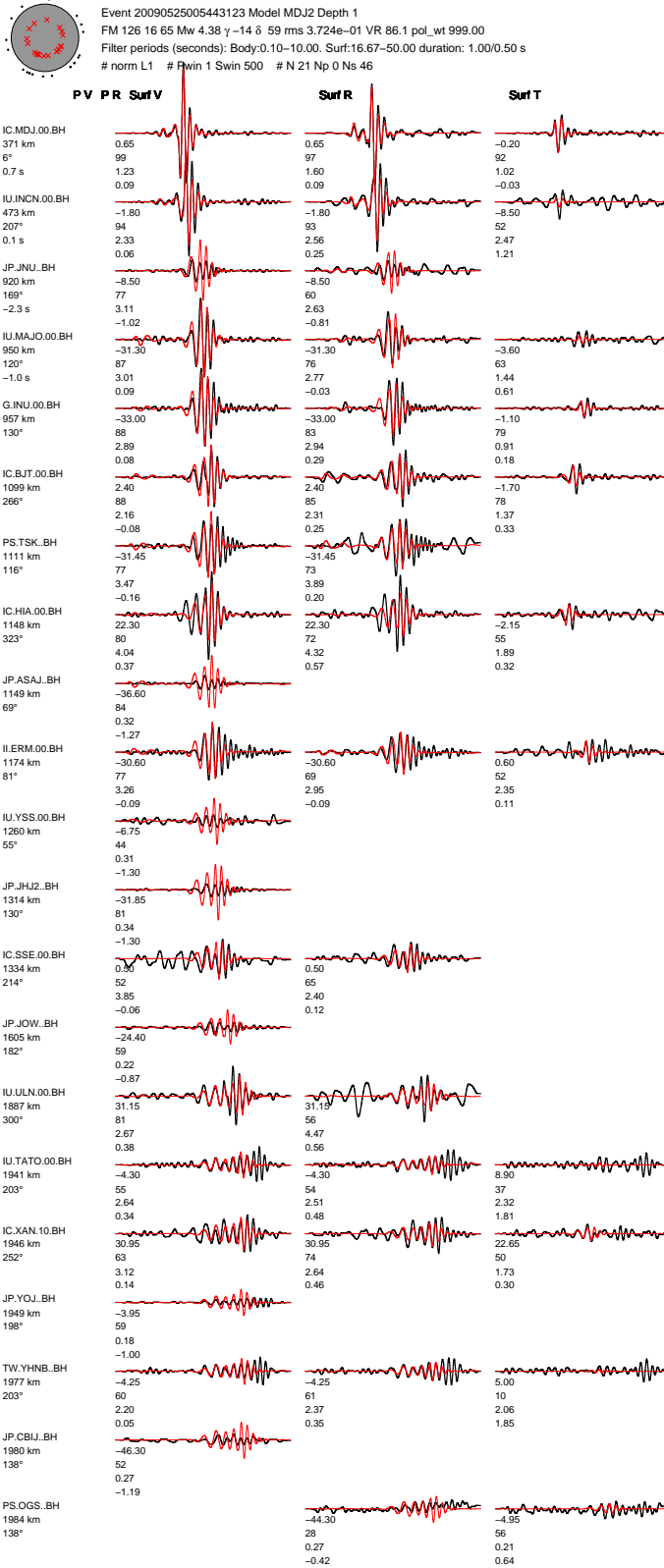


Figure D2: Best-fitting moment tensor and waveform fits for event NK2. Red = time-shifted synthetics, black = data. For each station, the three time windows are for Rayleigh waves (Surf V, Surf R) and for Love waves (Surf T). Numbers beneath each waveform pair are the time shift, the cross correlation maximum, the percentage of the misfit function, and the log amplitude ratio.

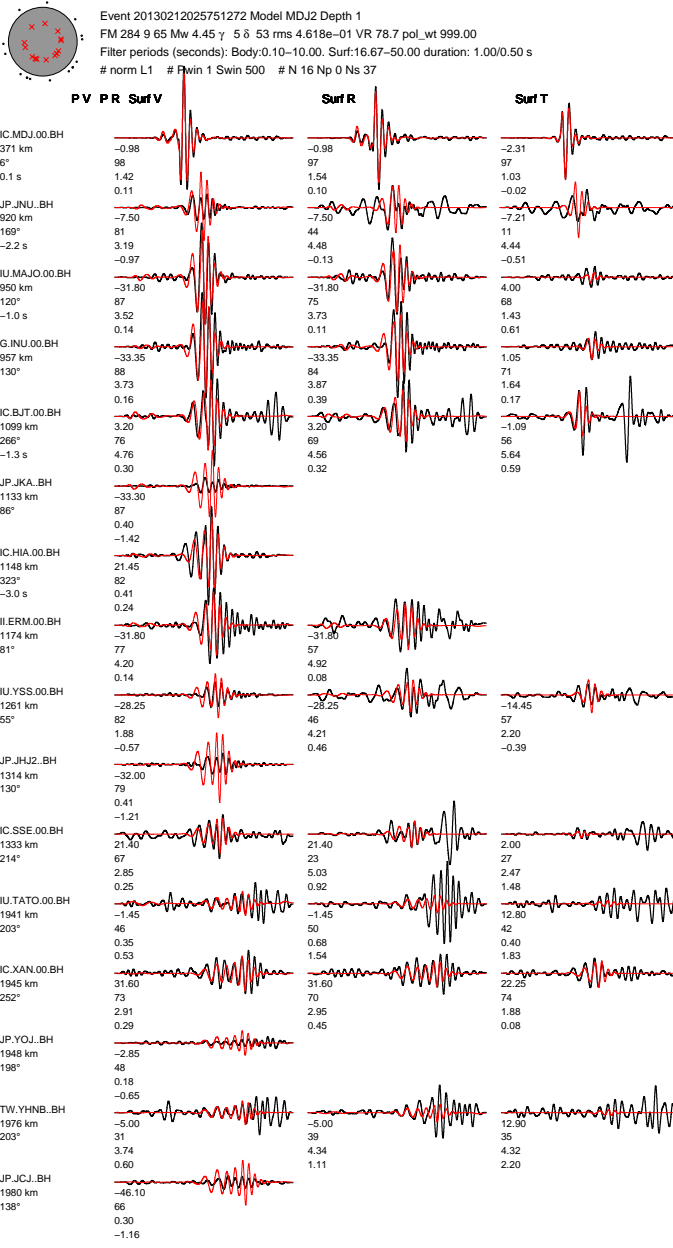


Figure D3: Best-fitting moment tensor and waveform fits for event NK3. Red = time-shifted synthetics, black = data. For each station, the three time windows are for Rayleigh waves (Surf V, Surf R) and for Love waves (Surf T). Numbers beneath each waveform pair are the time shift, the cross correlation maximum, the percentage of the misfit function, and the log amplitude ratio.

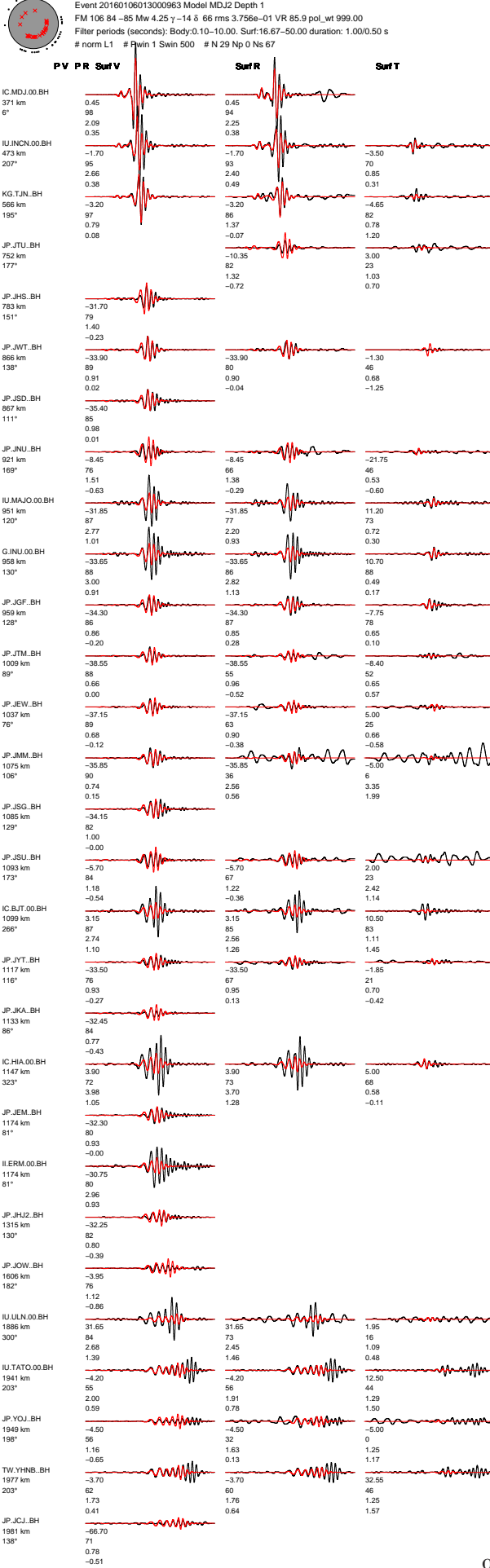


Figure D4: Best-fitting moment tensor and waveform fits for event NK4. Red = time-shifted synthetics, black = data. For each station, the three time windows are for Rayleigh waves (Surf V, Surf R) and for Love waves (Surf T). Numbers beneath each waveform pair are the time shift, the cross correlation maximum, the percentage of the misfit function, and the log amplitude ratio.

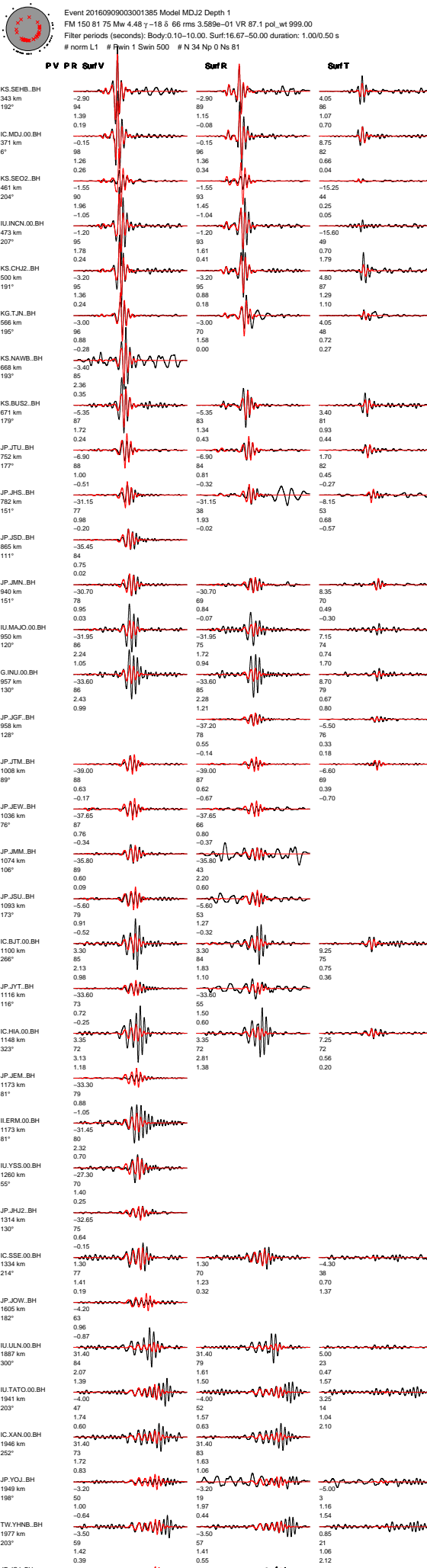


Figure D5: Best-fitting moment tensor and waveform fits for event NK5. Red = time-shifted synthetics, black = data. For each station, the three time windows are for Rayleigh waves (Surf V, Surf R) and for Love waves (Surf T). Numbers beneath each waveform pair are the time shift, the cross correlation maximum, the percentage of the misfit function, and the log amplitude ratio.

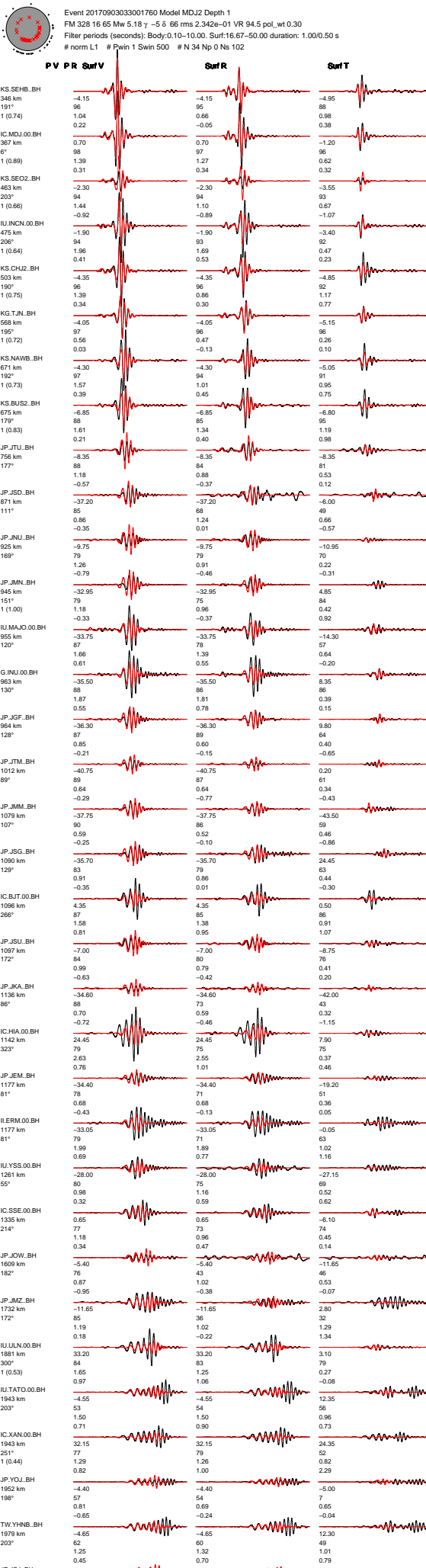


Figure D6: Best-fitting moment tensor and waveform fits for event NK6. Red = time-shifted synthetics, black = data. For each station, the three time windows are for Rayleigh waves (Surf V, Surf R) and for Love waves (Surf T). Numbers beneath each waveform pair are the time shift, the cross correlation maximum, the percentage of the misfit function, and the log amplitude ratio.

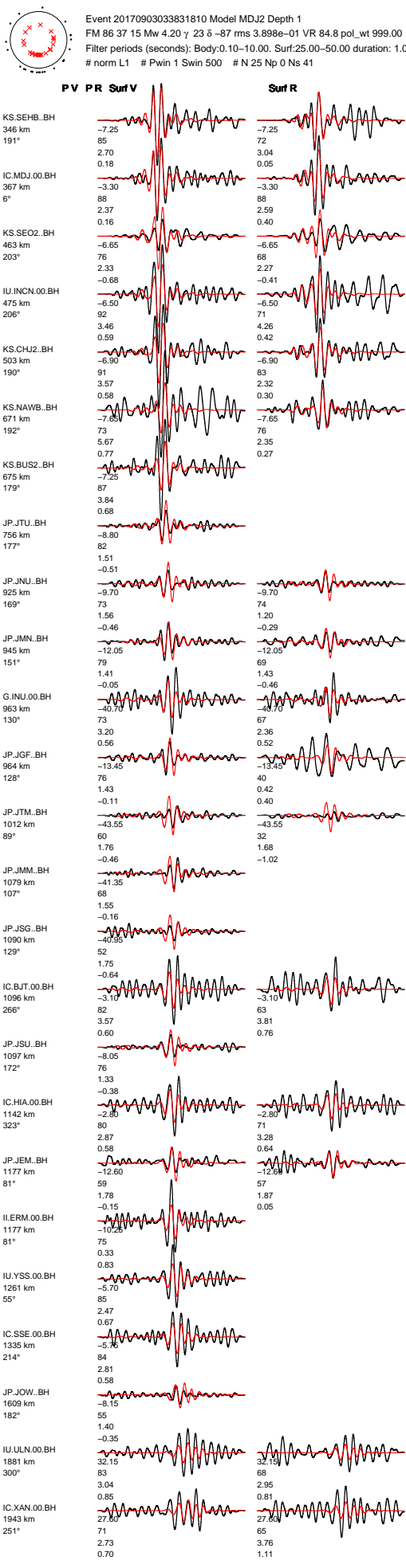


Figure D7: Best-fitting moment tensor and waveform fits for event NK6b. Red = time-shifted synthetics, black = data. For each station, the three time windows are for Rayleigh waves (Surf V, Surf R) and for Love waves (Surf T). Numbers beneath each waveform pair are the time shift, the cross correlation maximum, the percentage of the misfit function, and the log amplitude ratio.

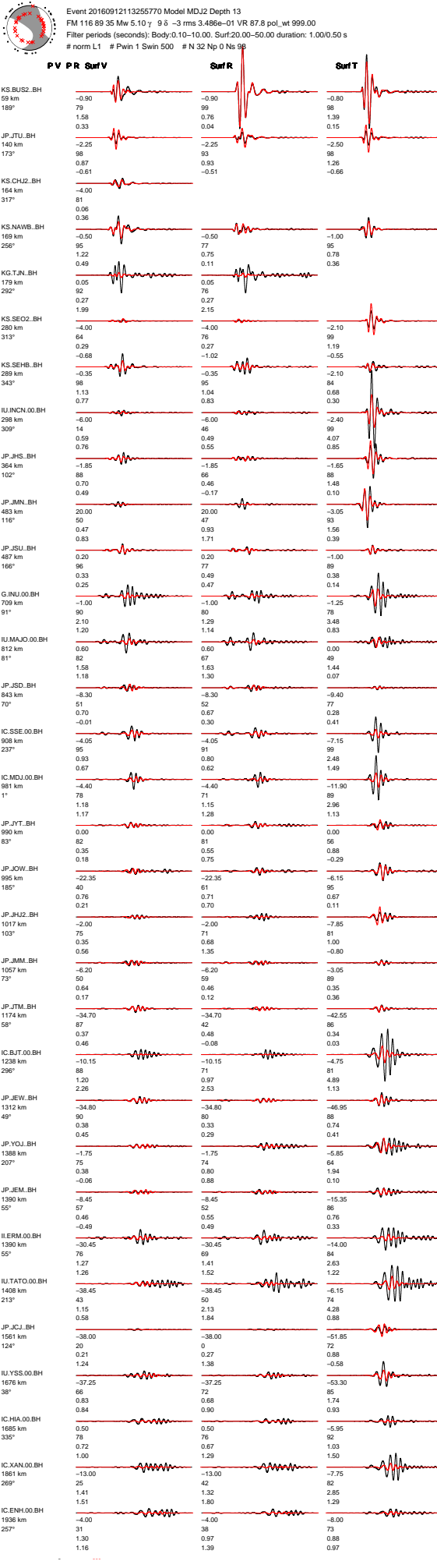


Figure D8: Best-fitting moment tensor and waveform fits for event EQ1. Red = time-shifted synthetics, black = data. For each station, the three time windows are for Rayleigh waves (Surf V, Surf R) and for Love waves (Surf T). Numbers beneath each waveform pair are the time shift, the cross correlation maximum, the percentage of the misfit function, and the log amplitude ratio.



Event 20171115052932820 Model MDJ2 Depth 3  
 FM 333 42 25 Mw 5.20  $\gamma$  0 8 -3 rms 3.346e-01 VR 88.8 pol\_wt 999.00  
 Filter periods (seconds): Body:0.10-10.00, Surf:20.00-50.00 duration: 1.00/0.50 s  
 # norm L1 # Pwin 1 Swin 400 # N 29 Np 0 Ns 82

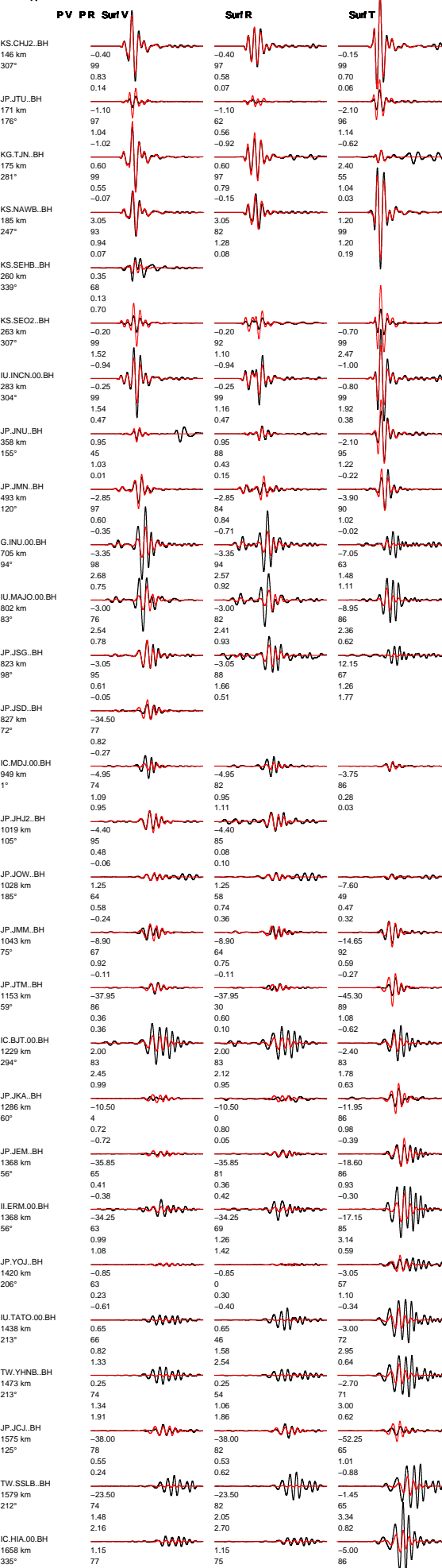
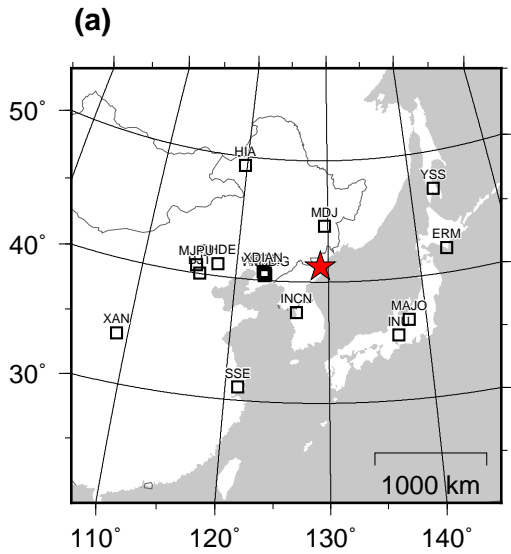


Figure D9: Best-fitting moment tensor and waveform fits for event EQ2. Red = time-shifted synthetics, black = data. For each station, the three time windows are for Rayleigh waves (Surf V, Surf R) and for Love waves (Surf T). Numbers beneath each waveform pair are the time shift, the cross correlation maximum, the percentage of the misfit function, and the log amplitude ratio.

Event 20061009013528000, M 3.81  
 Lon 129.1083, Lat 41.2874  
 Dep 1.0 km (inversion 1 km)  
 $\textcircled{O} (\gamma, \delta)_{\text{VR}}^{\max} = (-18^\circ, 66^\circ)$   $\blacksquare (\gamma, \delta)_p^{\max} = (-16^\circ, 55^\circ)$



(b) [No polarities]

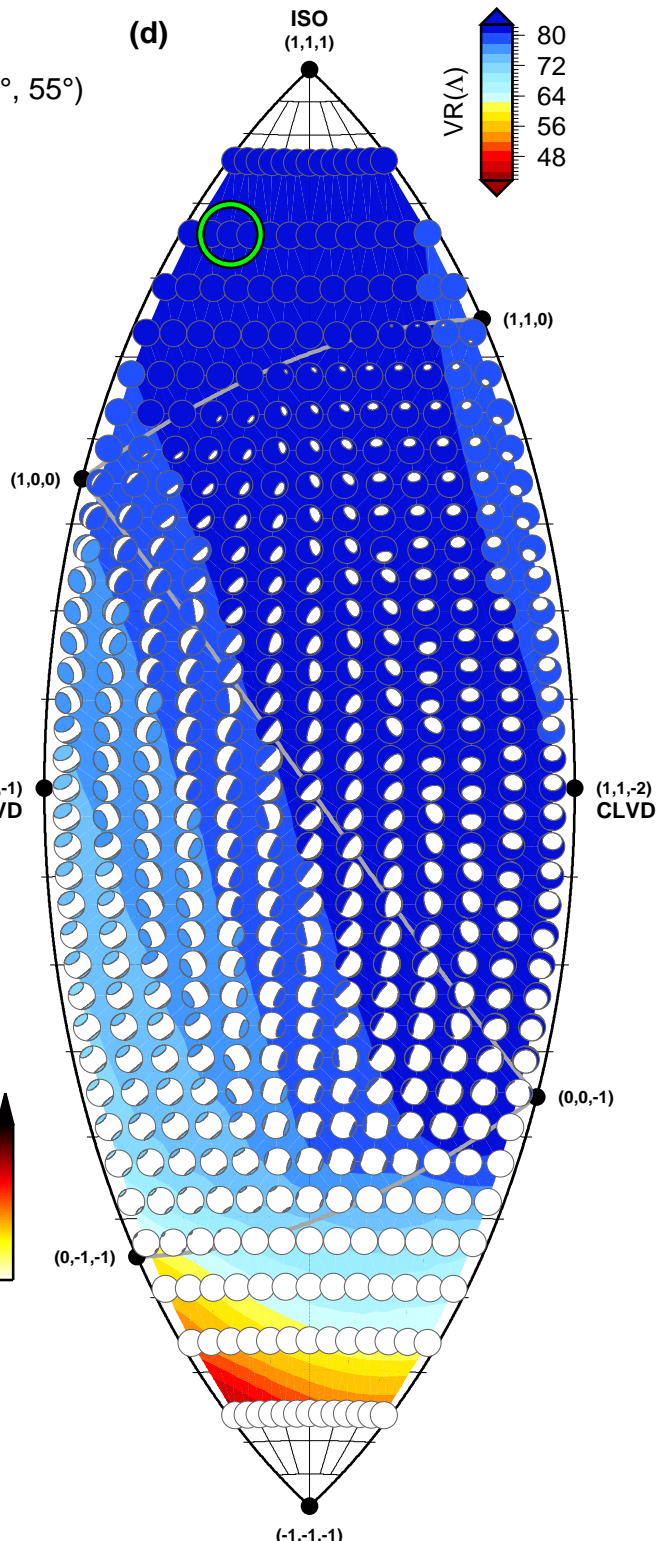
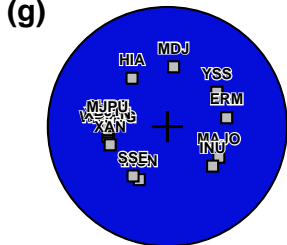
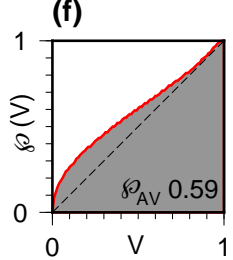
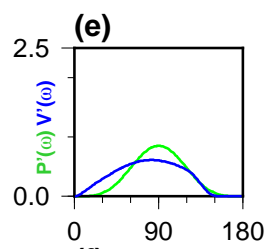
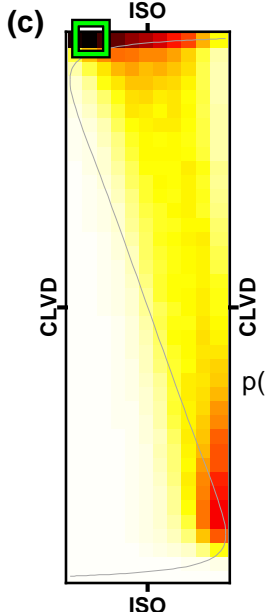
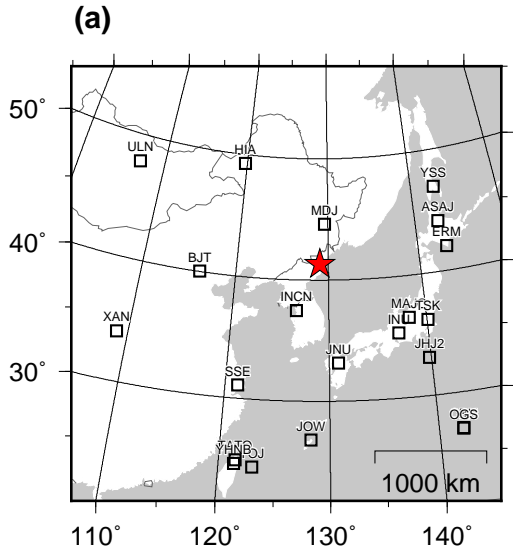


Figure D10: Uncertainty analysis for event NK1. See caption of Figure 4 for details.

Event 20090525005443123, M 4.38  
 Lon 129.0778, Lat 41.2943  
 Dep 1.0 km (inversion 1 km)  
 $\textcircled{O} (\gamma, \delta)_{\text{VR}}^{\max} = (-14^\circ, 59^\circ)$   $\blacksquare \gamma, \delta_p^{\max} = (-16^\circ, 55^\circ)$



(b) [No polarities]

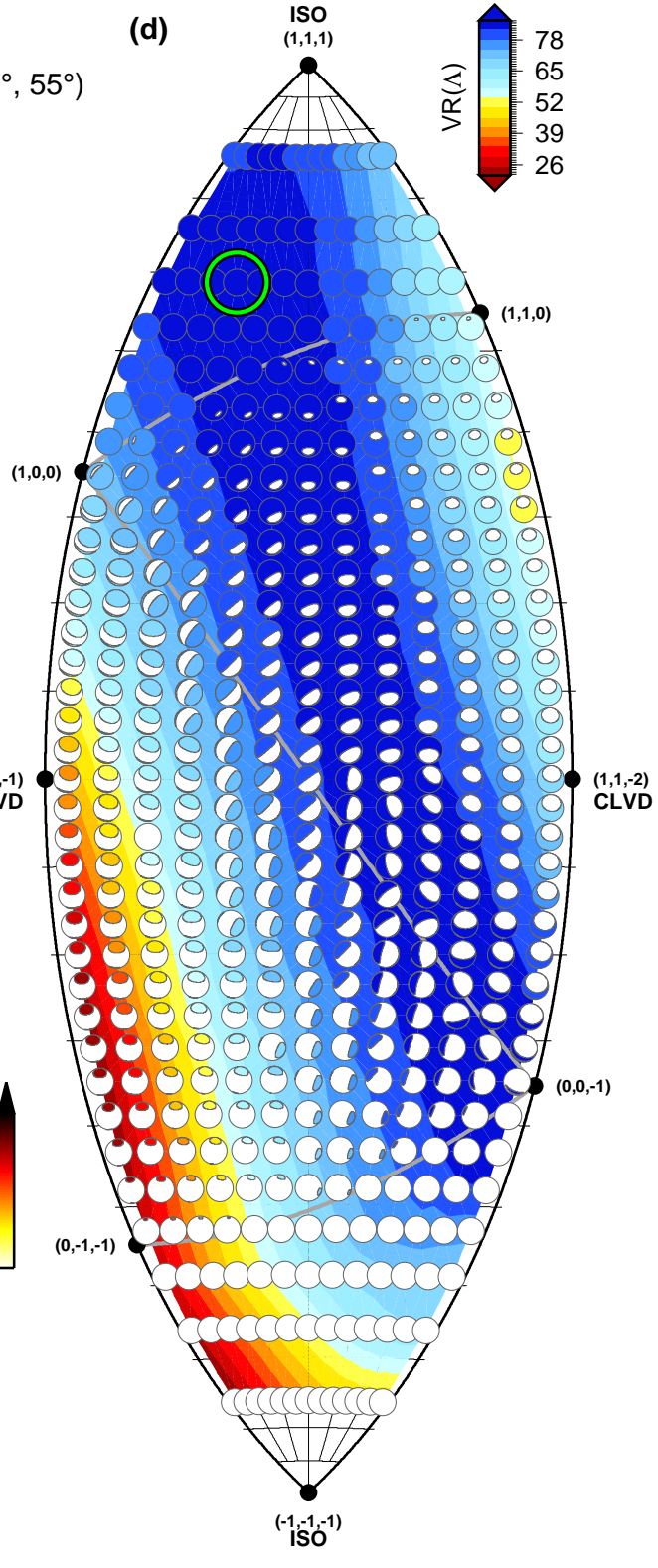
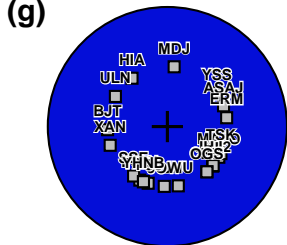
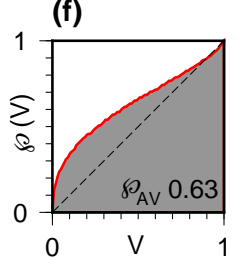
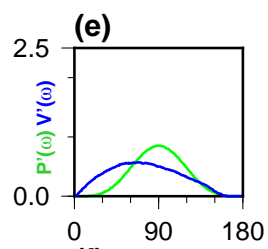
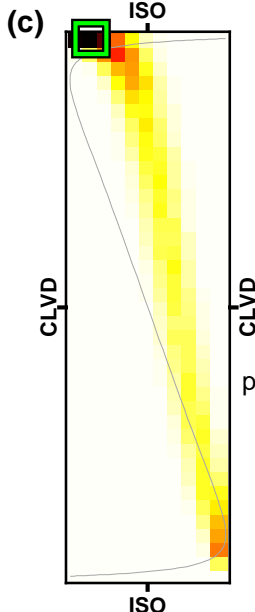
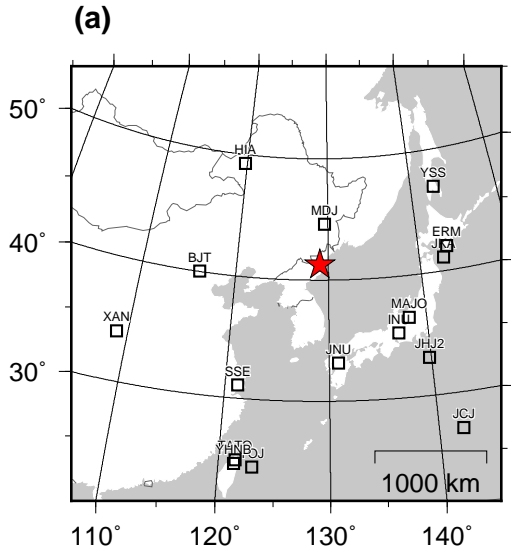


Figure D11: Uncertainty analysis for event NK2. See caption of Figure 4 for details.

Event 20130212025751272, M 4.45  
 Lon 129.0730, Lat 41.2921  
 Dep 1.0 km (inversion 1 km)  
 $\textcircled{O} (\gamma, \delta)_{\text{VR}}^{\max} = (5^\circ, 53^\circ)$     $\blacksquare \gamma, \delta_p^{\max} = (-16^\circ, 55^\circ)$



(b) [No polarities]

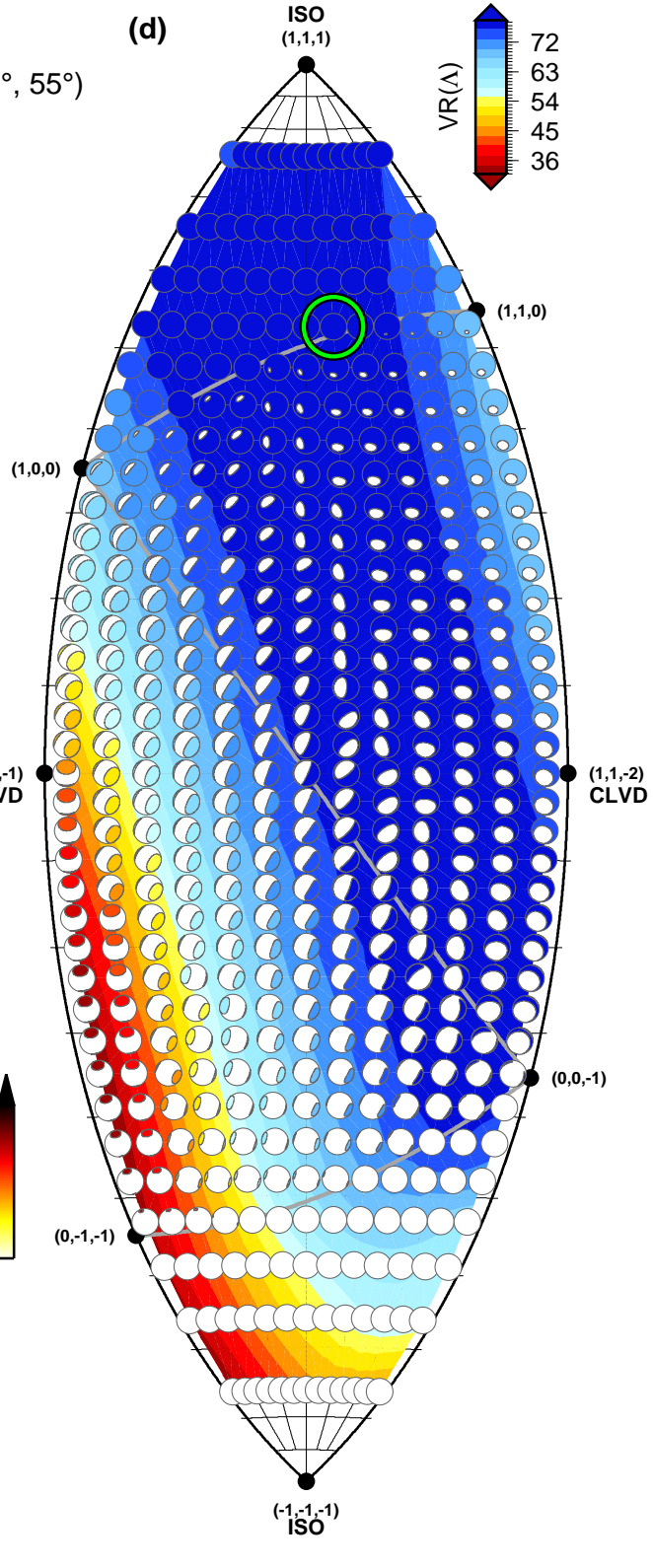
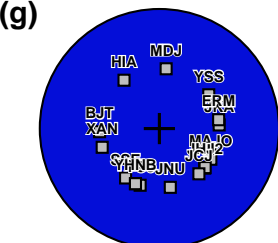
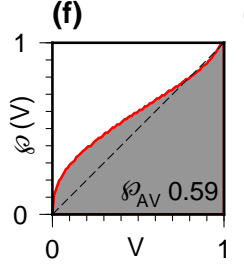
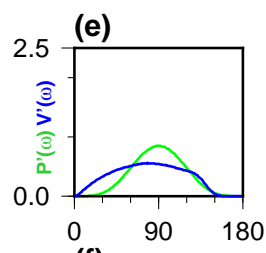
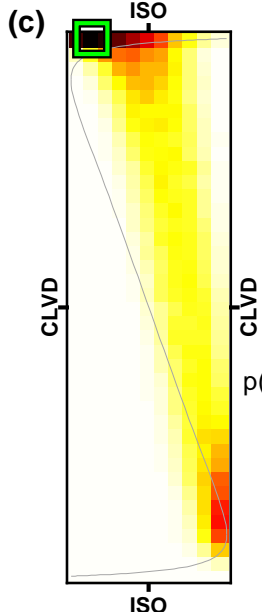
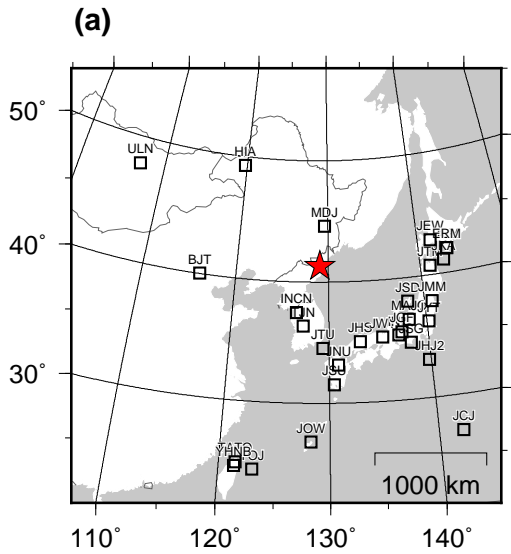


Figure D12: Uncertainty analysis for event NK3. See caption of Figure 4 for details.

Event 20160106013000963, M 4.25  
 Lon 129.0680, Lat 41.3001  
 Dep 1.0 km (inversion 1 km)  
 $\textcircled{O} (\gamma, \delta)_{\text{VR}}^{\max} = (-14^\circ, 66^\circ)$   $\blacksquare (\gamma, \delta)_p^{\max} = (11^\circ, 55^\circ)$



(b) [No polarities]

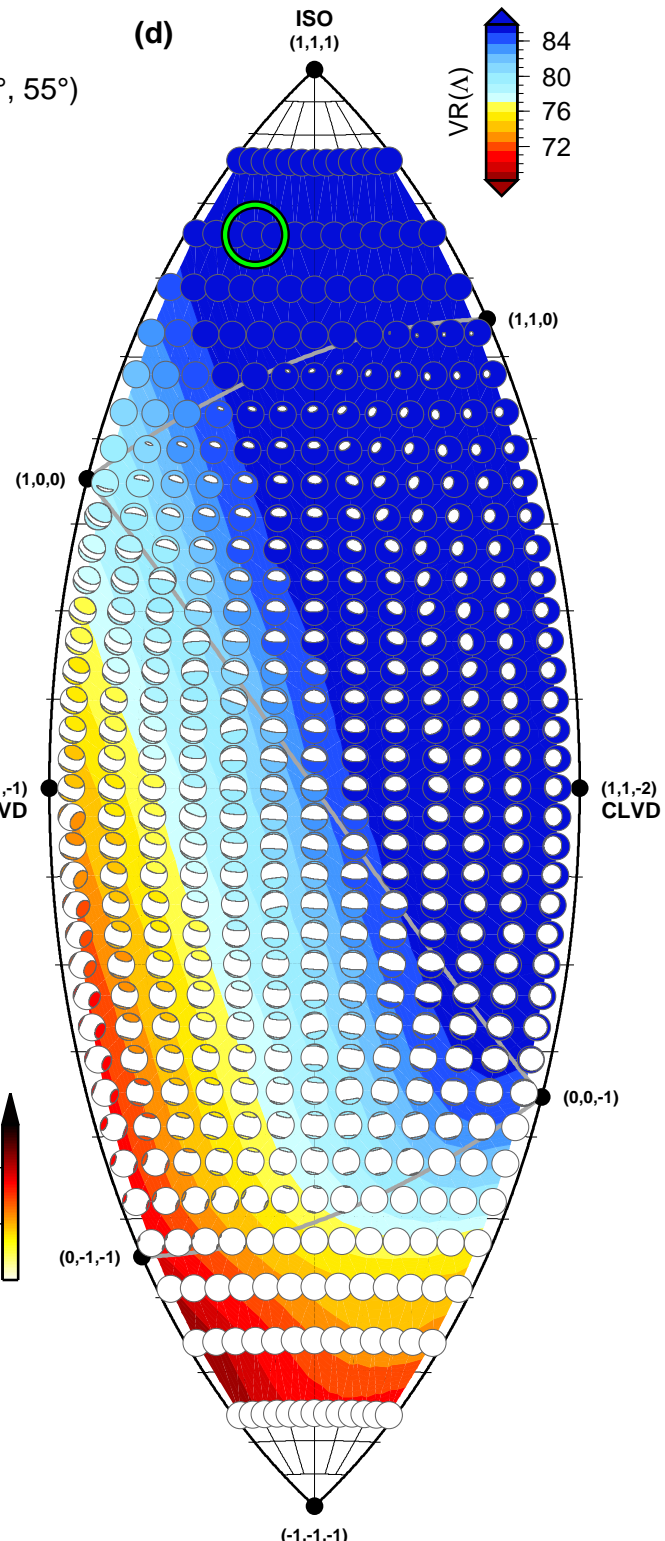
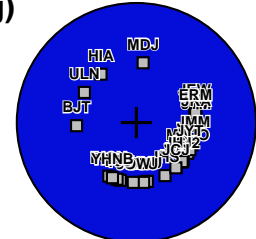
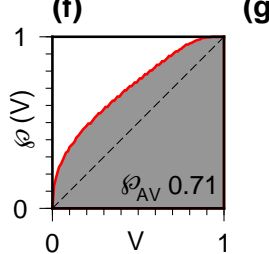
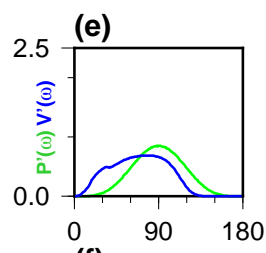
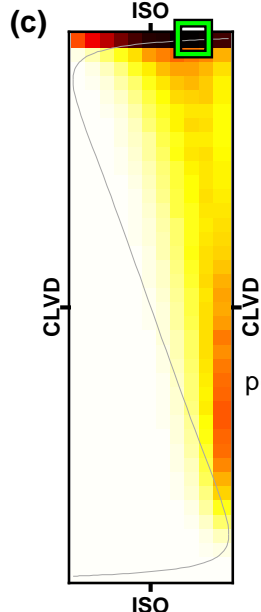
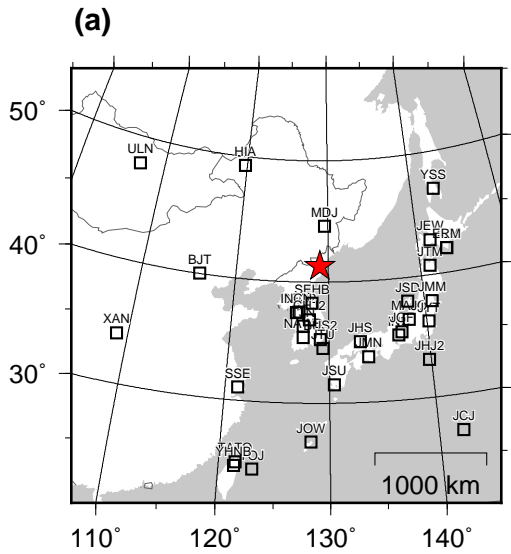


Figure D13: Uncertainty analysis for event NK4. See caption of Figure 4 for details.

Event 20160909003001385, M 4.48  
 Lon 129.0804, Lat 41.2976  
 Dep 1.0 km (inversion 1 km)  
 $\textcircled{O} (\gamma, \delta)_{\text{VR}}^{\max} = (-18^\circ, 66^\circ)$   $\blacksquare (\gamma, \delta)_p^{\max} = (-3^\circ, 55^\circ)$



(b) [No polarities]

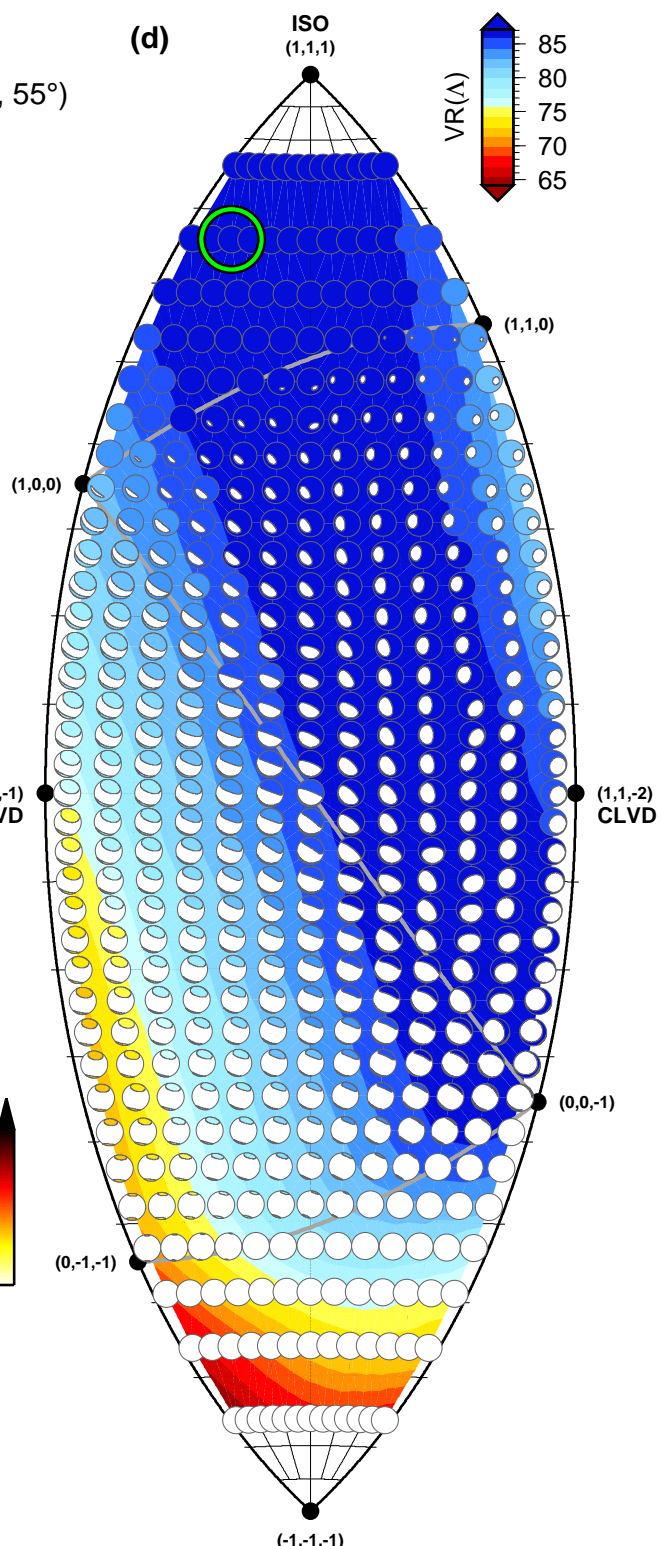
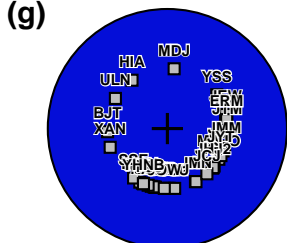
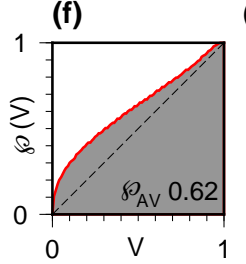
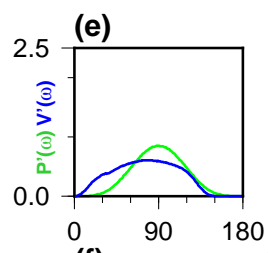
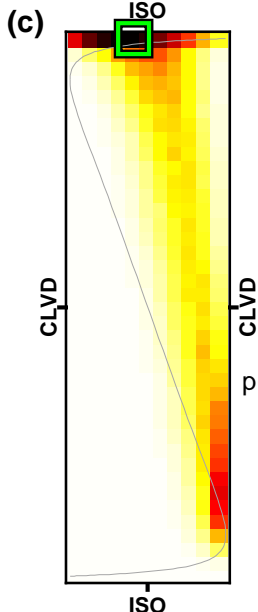
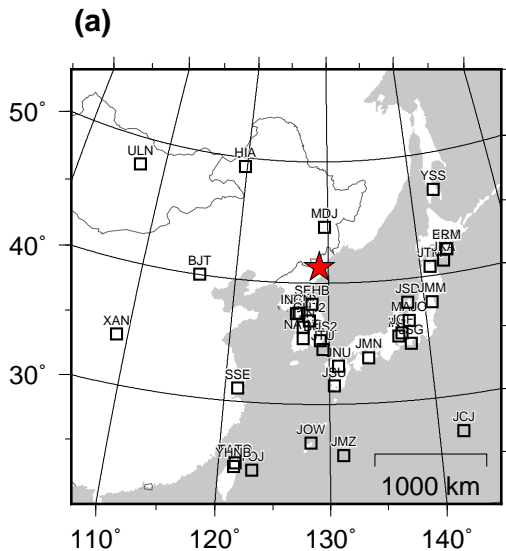


Figure D14: Uncertainty analysis for event NK5. See caption of Figure 4 for details.

Event 20170903033001760, M 5.18  
 Lon 129.0297, Lat 41.3324  
 Dep 0.0 km (inversion 1 km)  
 $\text{O}(\gamma, \delta)_{\text{VR}}^{\max} = (-5^\circ, 66^\circ)$   $\text{O}(\gamma, \delta)_p^{\max} = (-7^\circ, 55^\circ)$



(b) [No polarities]

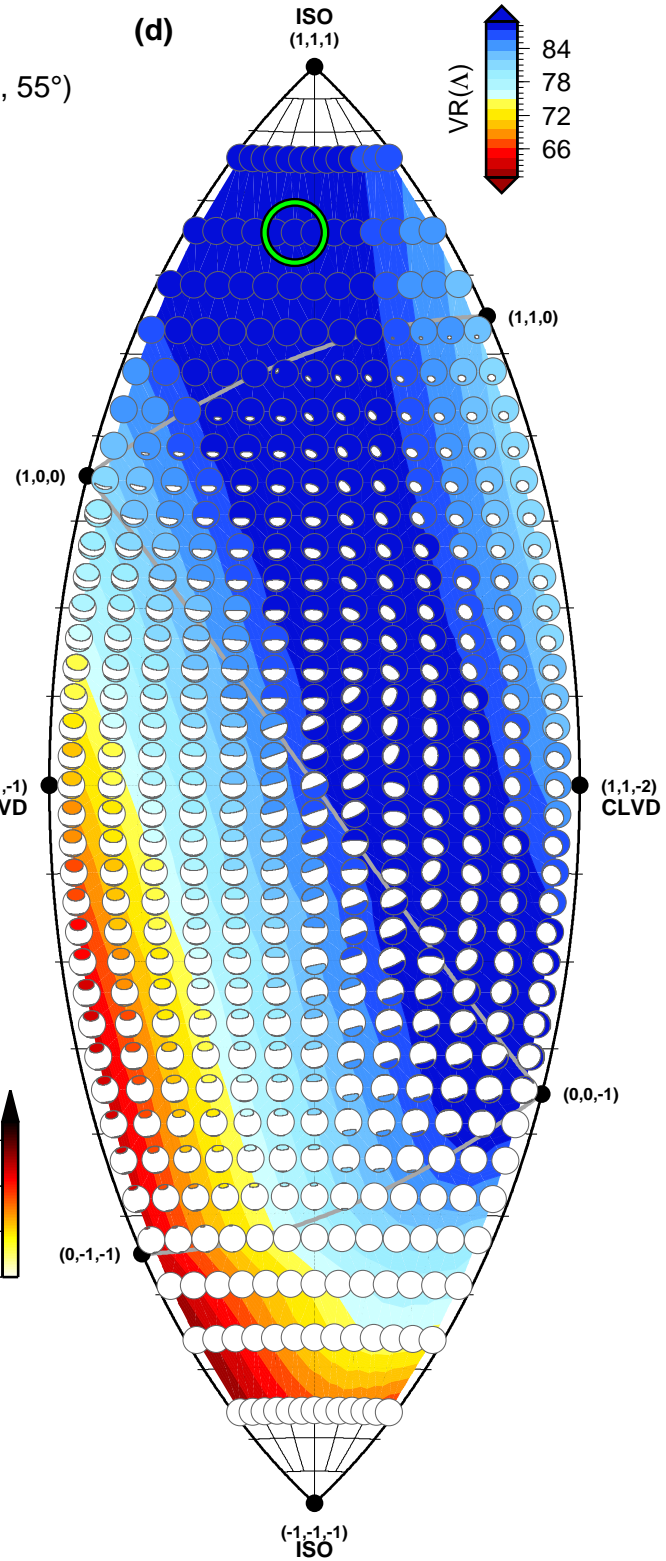
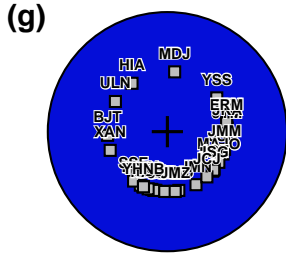
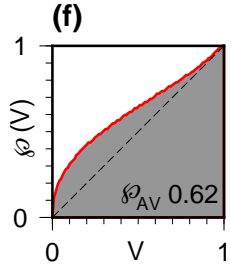
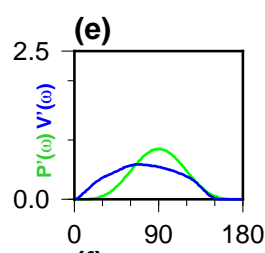
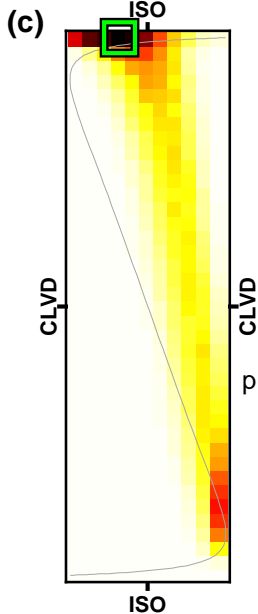
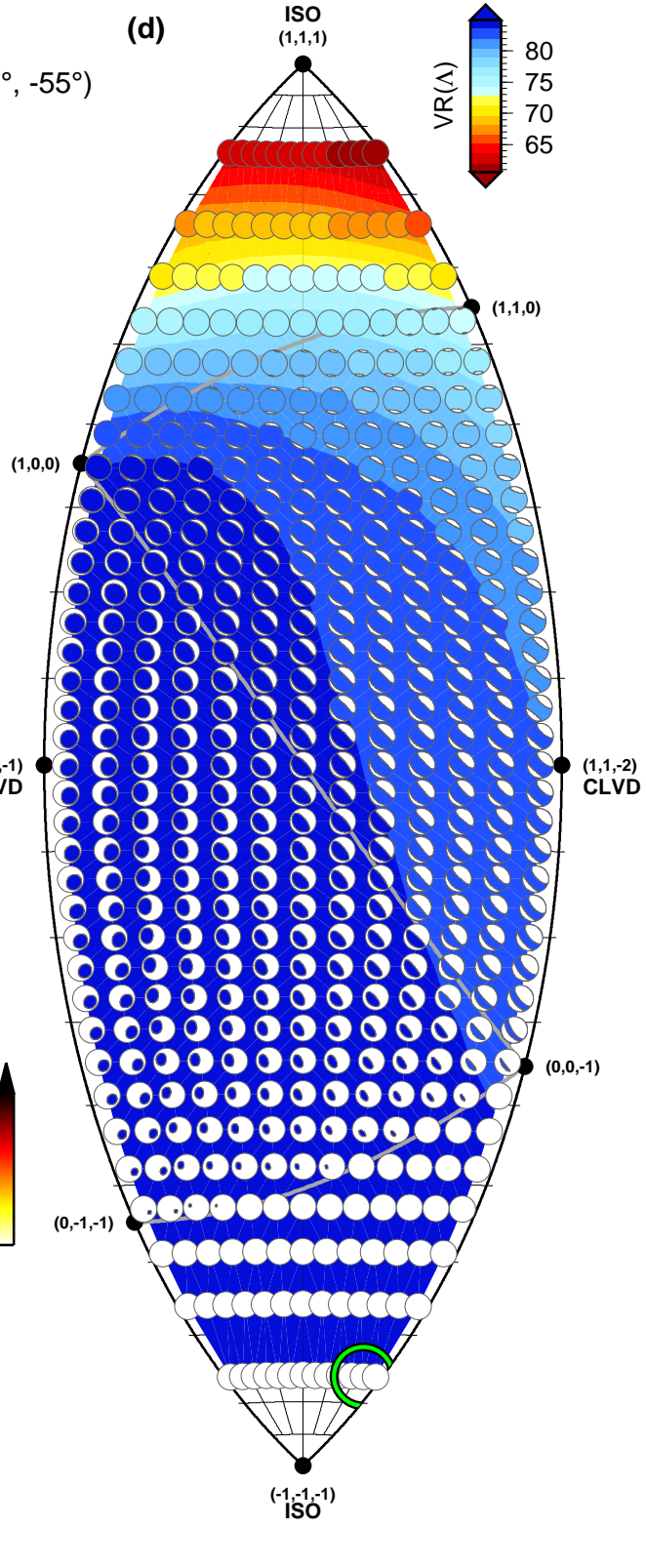
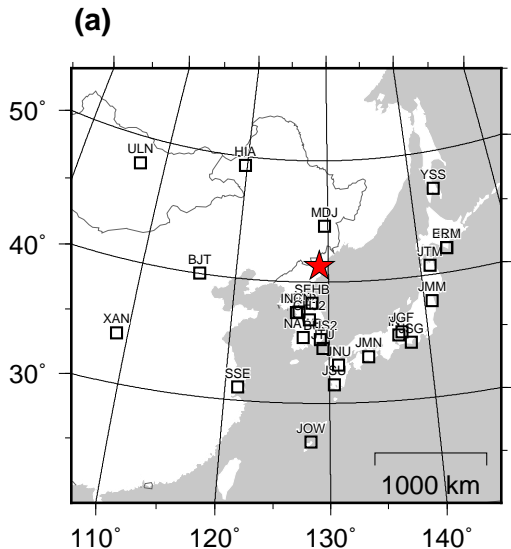


Figure D15: Uncertainty analysis for event NK6. See caption of Figure 4 for details. This is the same as Figure 4, but here no polarities were used. This figure is also displayed in Figure S5.

Event 20170903033831810, M 4.20  
 Lon 129.0310, Lat 41.3340  
 Dep 0.0 km (inversion 1 km)  
 $\textcircled{O} (\gamma, \delta)_{\text{VR}}^{\max} = (23^\circ, -76^\circ)$   $\blacksquare (\gamma, \delta)_p^{\max} = (-22^\circ, -55^\circ)$



(b) [No polarities]

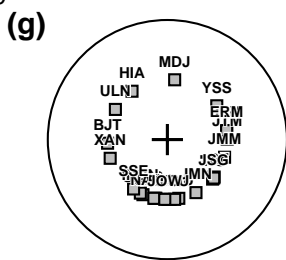
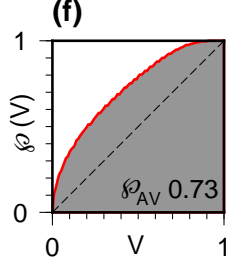
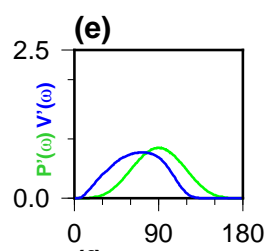
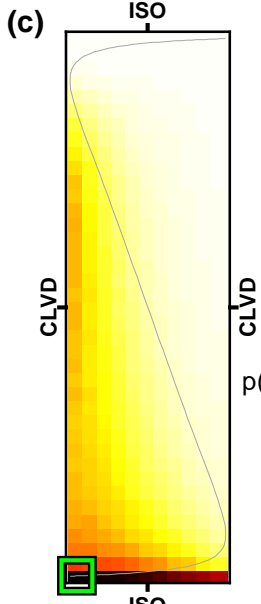
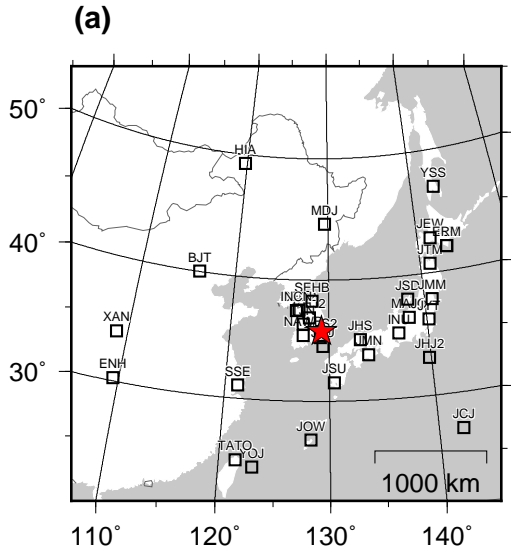


Figure D16: Uncertainty analysis for event NK6b. See caption of Figure 4 for details.

Event 20160912113255770, M 5.10  
 Lon 129.2162, Lat 35.7808  
 Dep 13.0 km (inversion 13 km)  
 $\textcircled{O} (\gamma, \delta)_{\text{VR}}^{\max} = (9^\circ, -3^\circ)$     $\blacksquare \gamma, \delta_p^{\max} = (16^\circ, 0^\circ)$



(b) [No polarities]

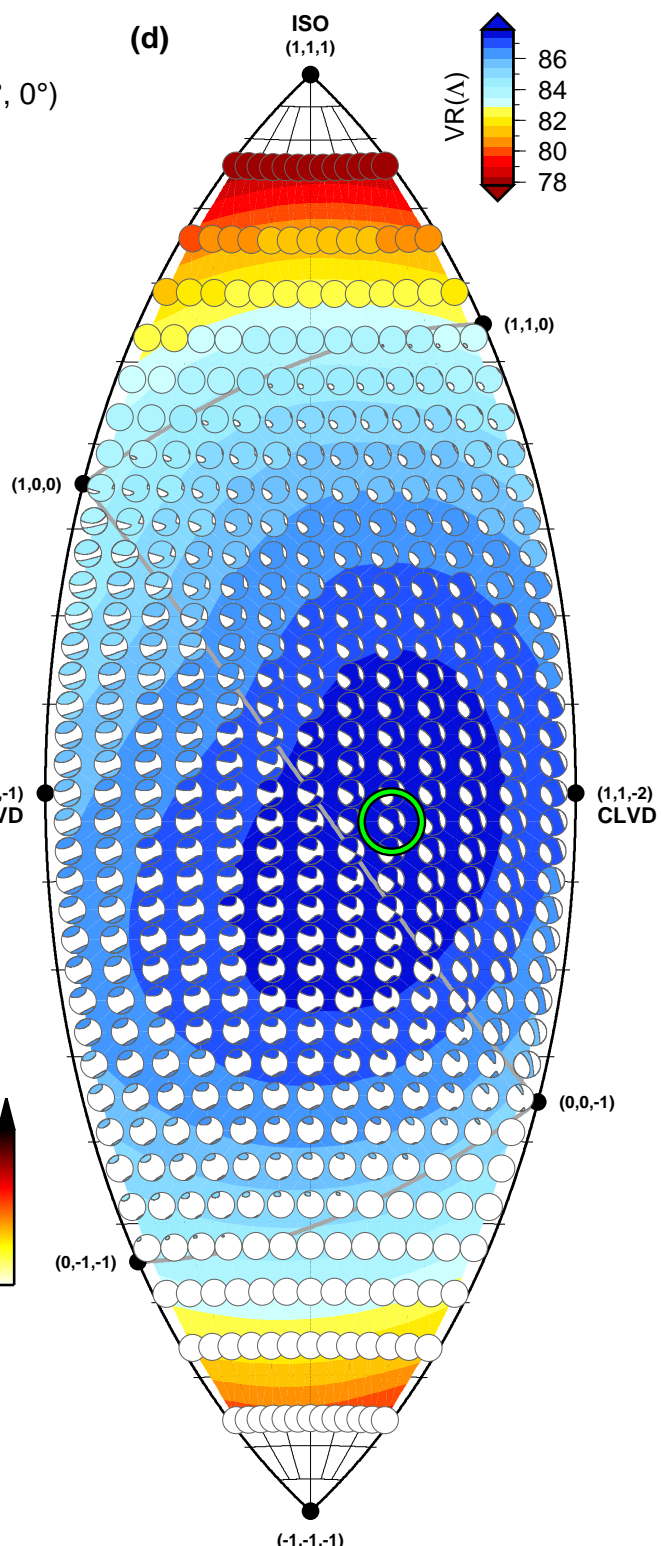
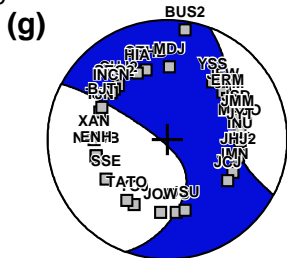
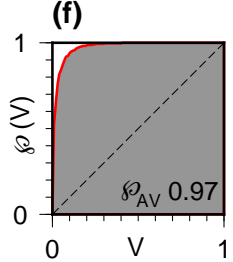
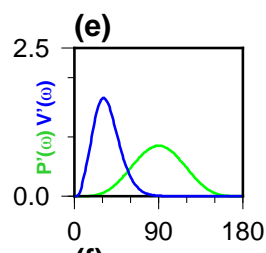
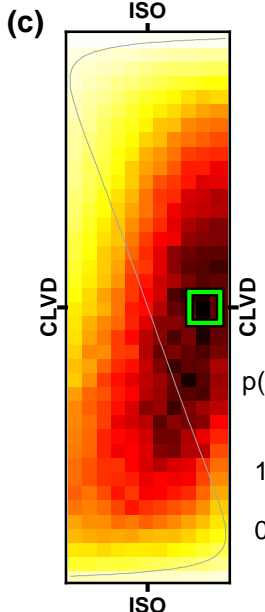
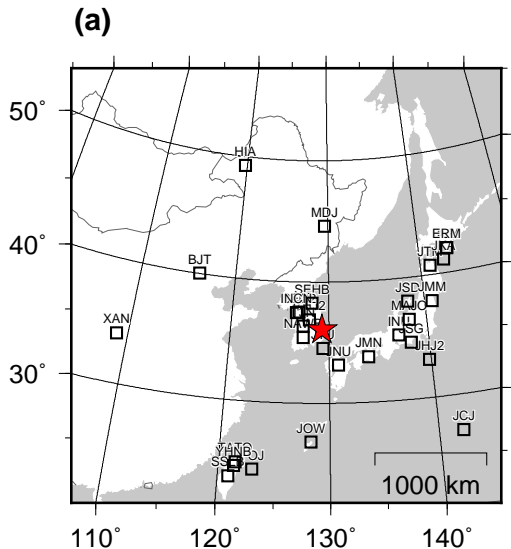


Figure D17: Uncertainty analysis for event EQ1. See caption of Figure 4 for details.

Event 20171115052932820, M 5.20  
 Lon 129.2800, Lat 36.0735  
 Dep 10.0 km (inversion 3 km)  
 $\textcircled{O} (\gamma, \delta)_{\text{VR}}^{\max} = (0^\circ, -3^\circ)$     $\blacksquare \gamma, \delta_p^{\max} = (-16^\circ, -45^\circ)$



(b) [No polarities]

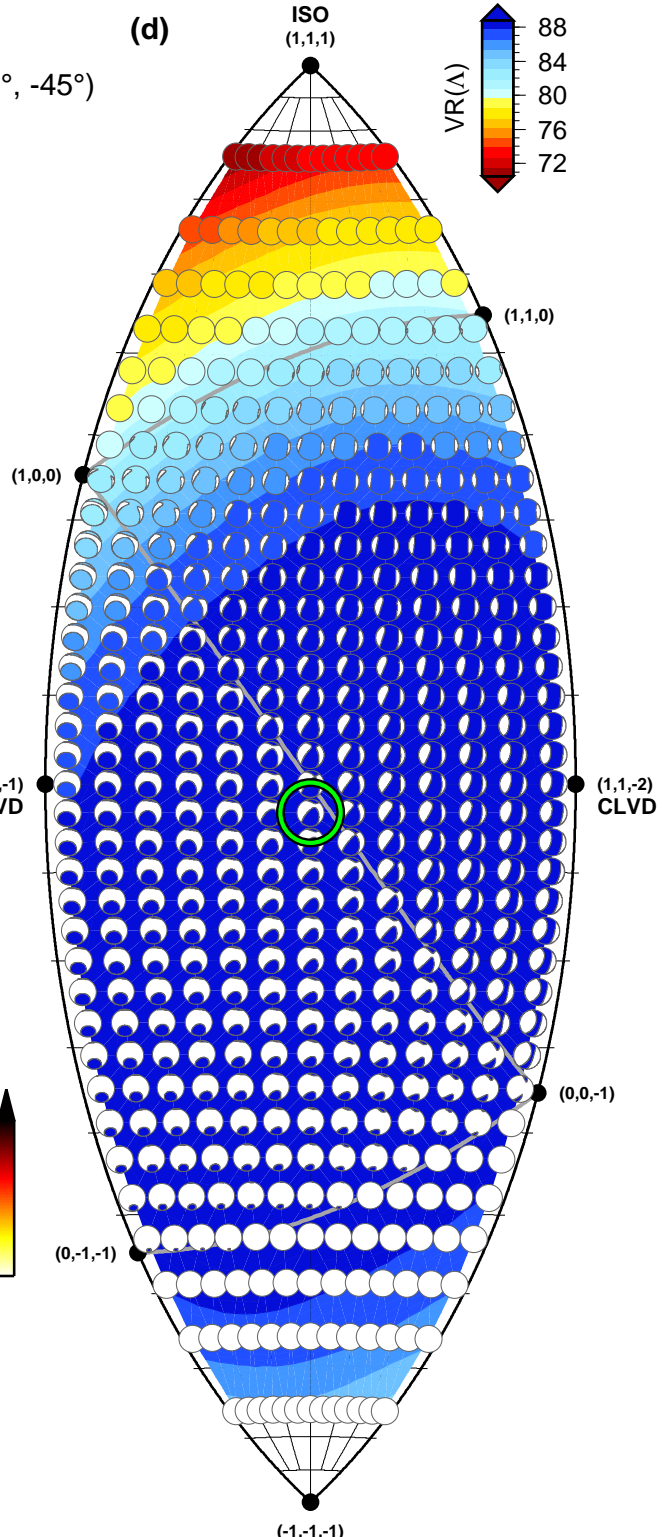
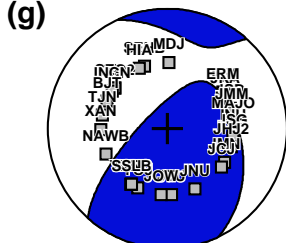
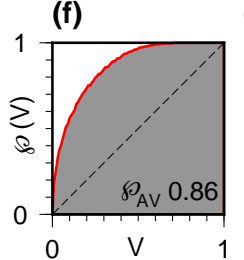
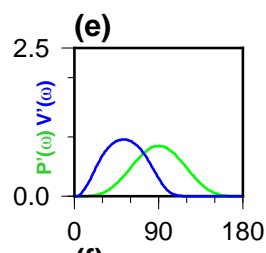
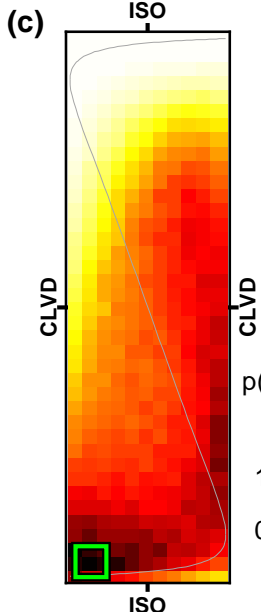


Figure D18: Uncertainty analysis for event EQ2. See caption of Figure 4 for details.

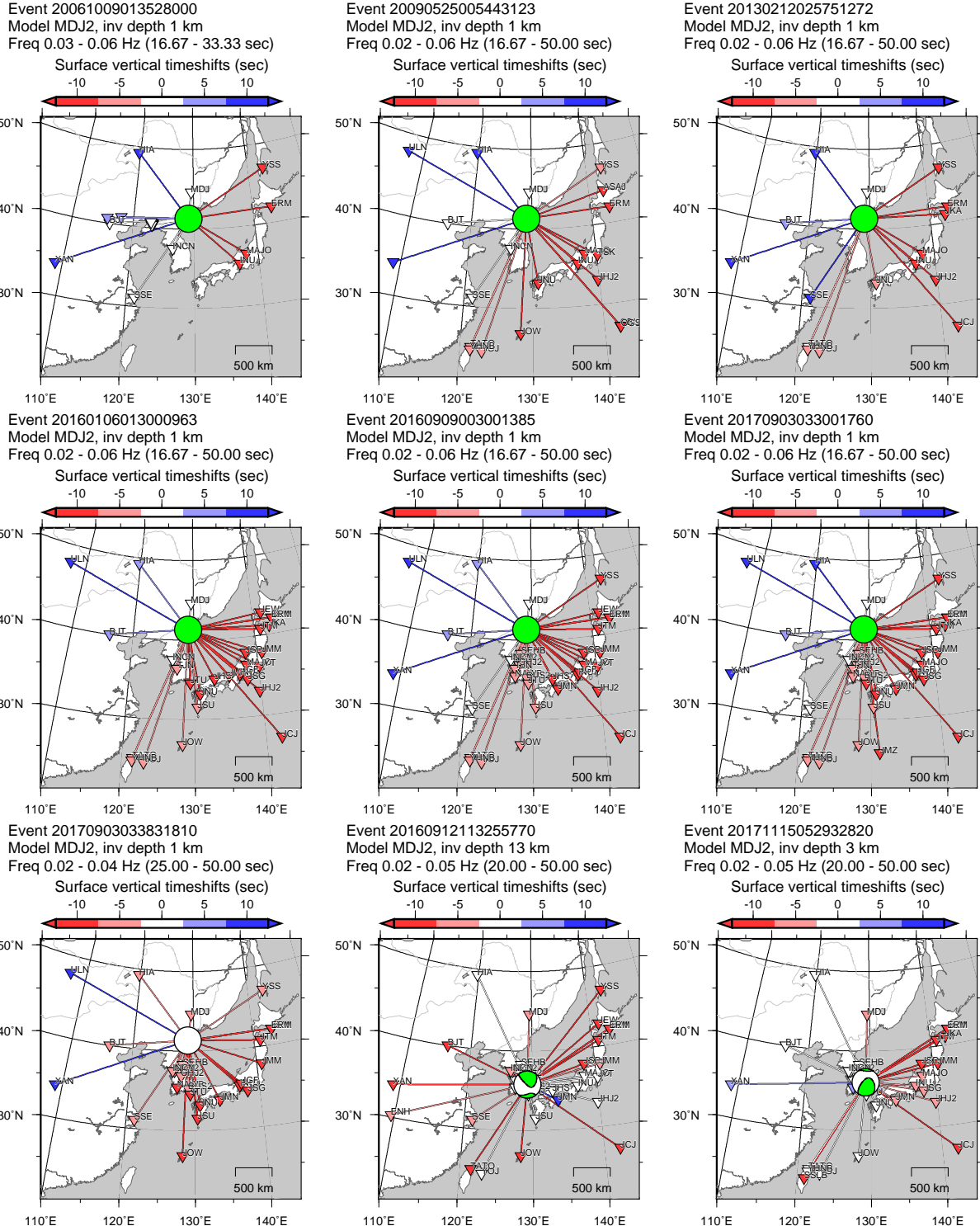


Figure D19: Rayleigh wave time shifts for all nine events.

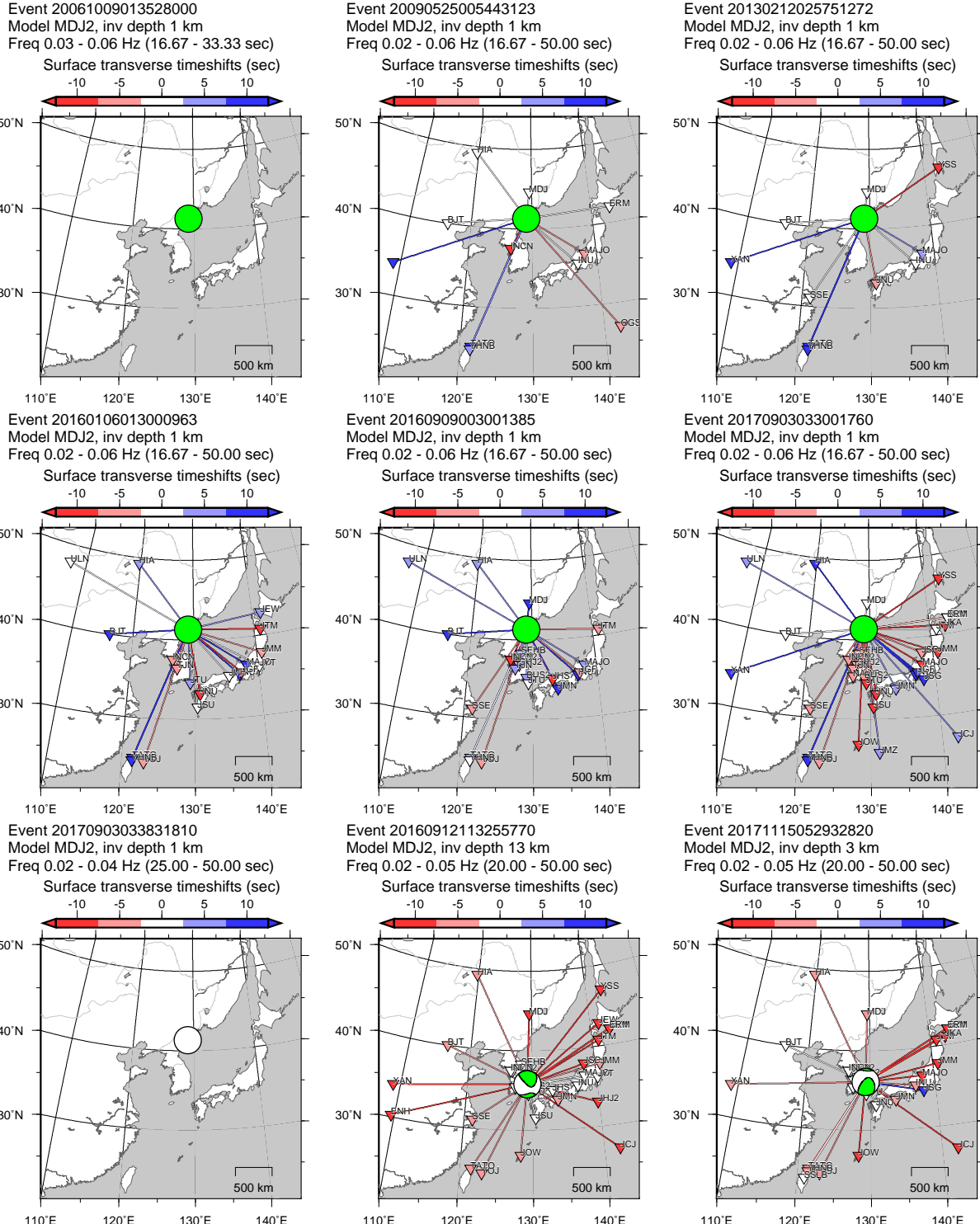


Figure D20: Love wave time shifts for all nine events.

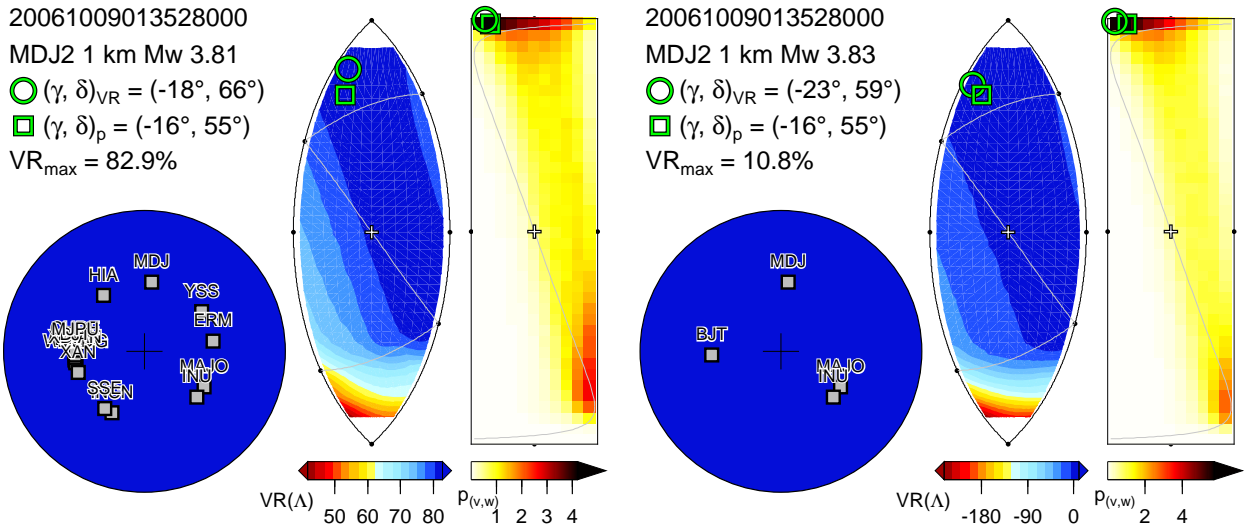


Figure D21: Moment tensor and uncertainties for NK1 using four stations (left) and all stations (right). The beachball is the best-fitting moment tensor, indicated by the white circle on the lune plot. The lune shows the variance reduction  $VR(\Lambda)$ . The  $vw$ -rectangle shows  $p(v,w)$ , the probability density for source type; the maximum of  $p(v,w)$  is denoted by the green circle.

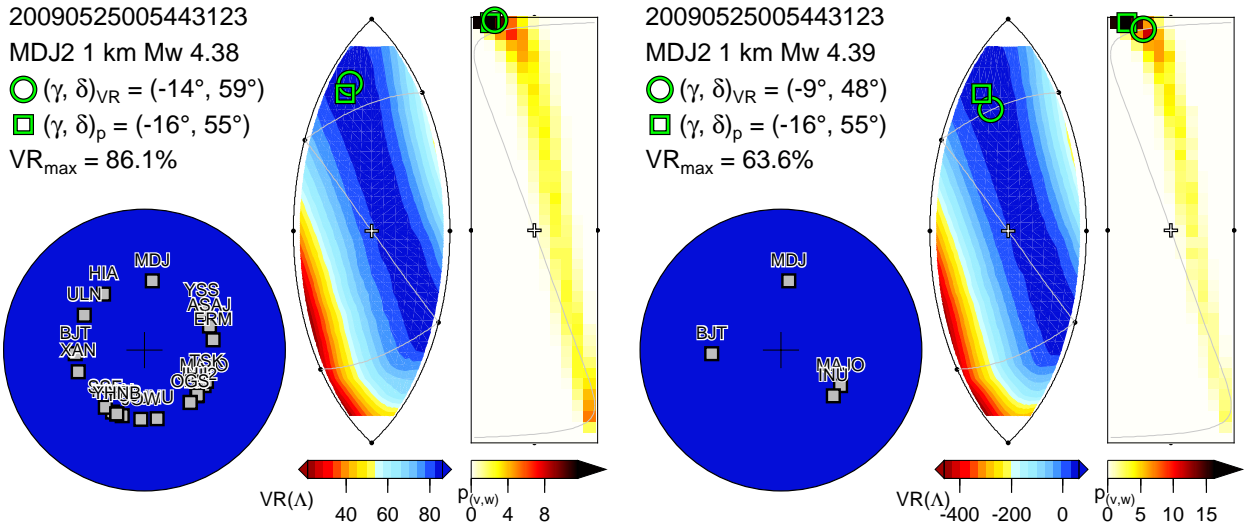


Figure D22: Moment tensor and uncertainties for NK2 using four stations (left) and all stations (right). The beachball is the best-fitting moment tensor, indicated by the white circle on the lune plot. The lune shows the variance reduction  $VR(\Lambda)$ . The  $vw$ -rectangle shows  $p(v,w)$ , the probability density for source type; the maximum of  $p(v,w)$  is denoted by the green circle.

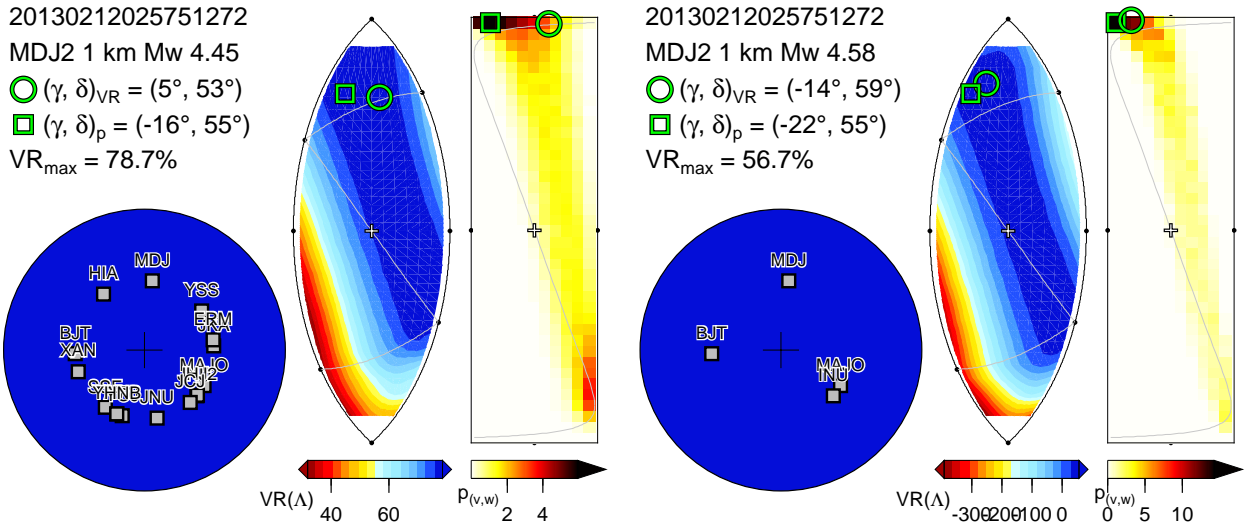


Figure D23: Moment tensor and uncertainties for NK3 using four stations (left) and all stations (right). The beachball is the best-fitting moment tensor, indicated by the white circle on the lune plot. The lune shows the variance reduction  $VR(\Lambda)$ . The  $vw$ -rectangle shows  $p(v,w)$ , the probability density for source type; the maximum of  $p(v,w)$  is denoted by the green circle.

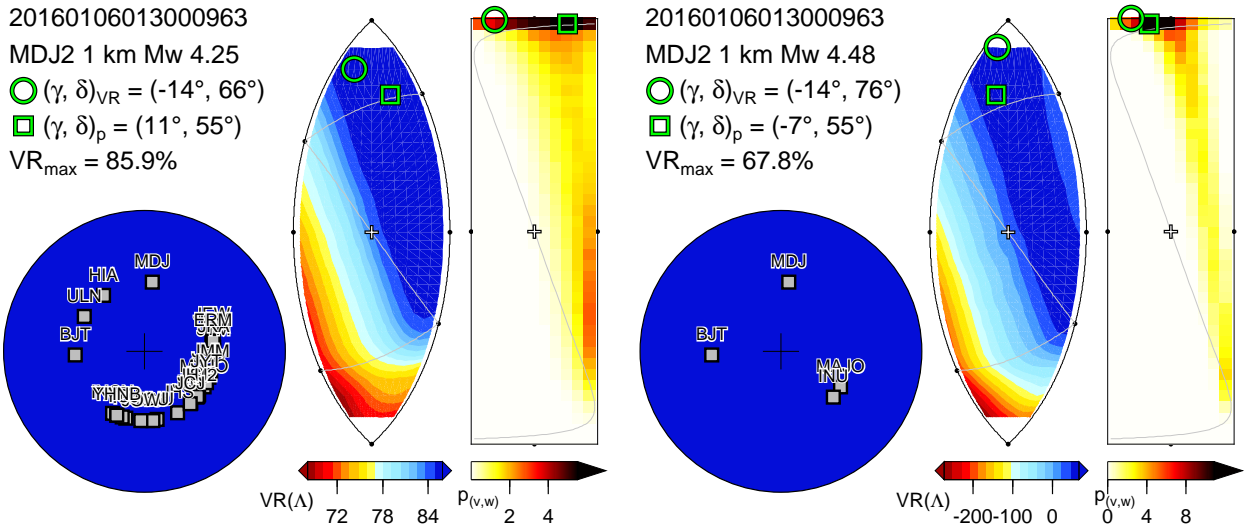


Figure D24: Moment tensor and uncertainties for NK4 using four stations (left) and all stations (right). The beachball is the best-fitting moment tensor, indicated by the white circle on the lune plot. The lune shows the variance reduction  $VR(\Lambda)$ . The  $vw$ -rectangle shows  $p(v, w)$ , the probability density for source type; the maximum of  $p(v, w)$  is denoted by the green circle.

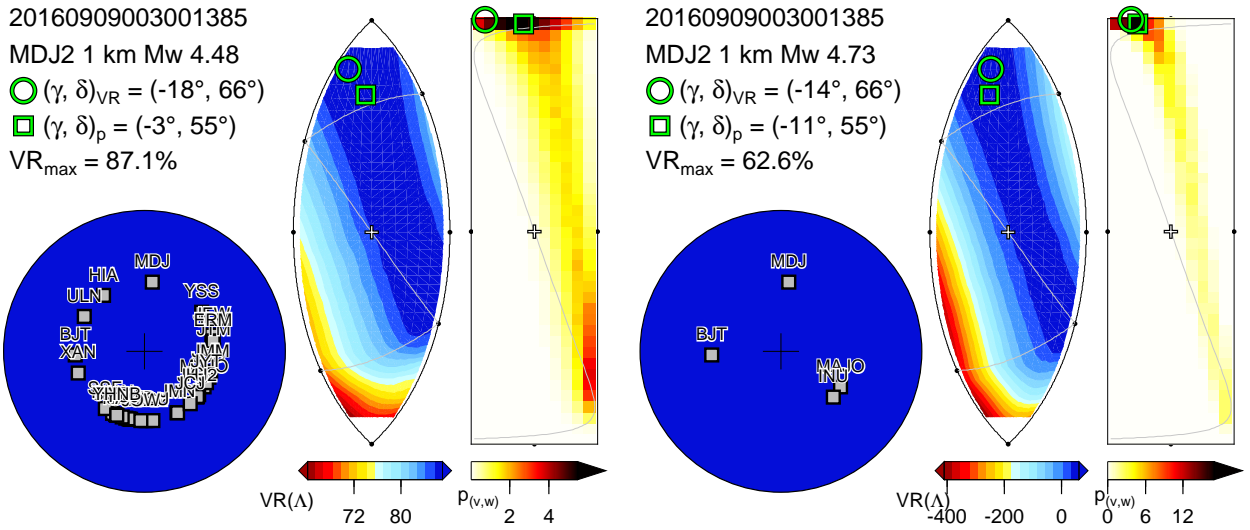


Figure D25: Moment tensor and uncertainties for NK5 using four stations (left) and all stations (right). The beachball is the best-fitting moment tensor, indicated by the white circle on the lune plot. The lune shows the variance reduction  $VR(\Lambda)$ . The  $vw$ -rectangle shows  $p(v,w)$ , the probability density for source type; the maximum of  $p(v,w)$  is denoted by the green circle.

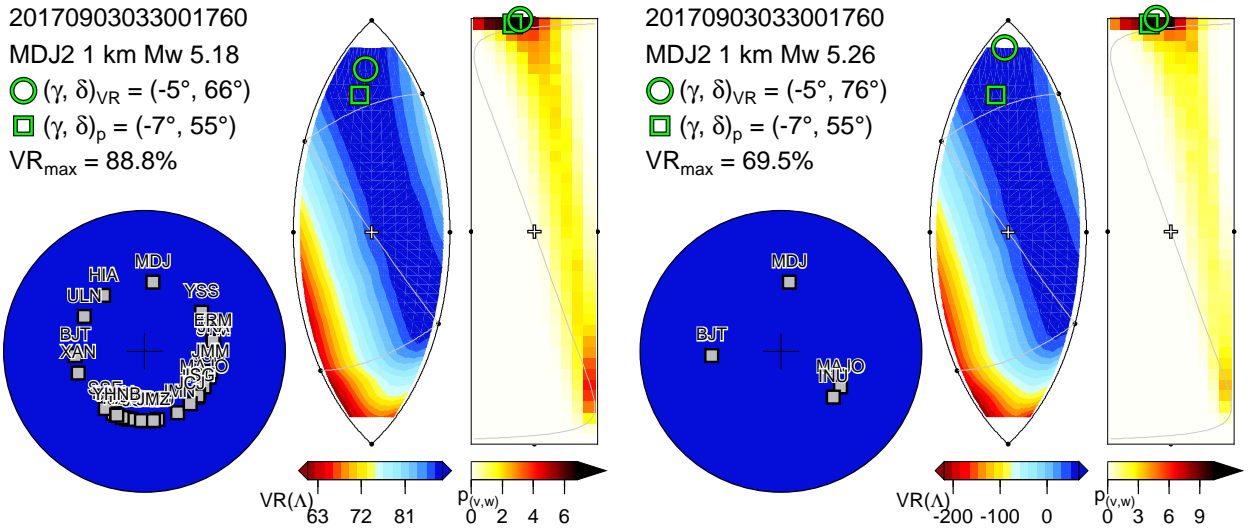


Figure D26: Moment tensor and uncertainties for NK6 using four stations (left) and all stations (right). The beachball is the best-fitting moment tensor, indicated by the white circle on the lune plot. The lune shows the variance reduction  $VR(\Lambda)$ . The  $vw$ -rectangle shows  $p(v, w)$ , the probability density for source type; the maximum of  $p(v, w)$  is denoted by the green circle.

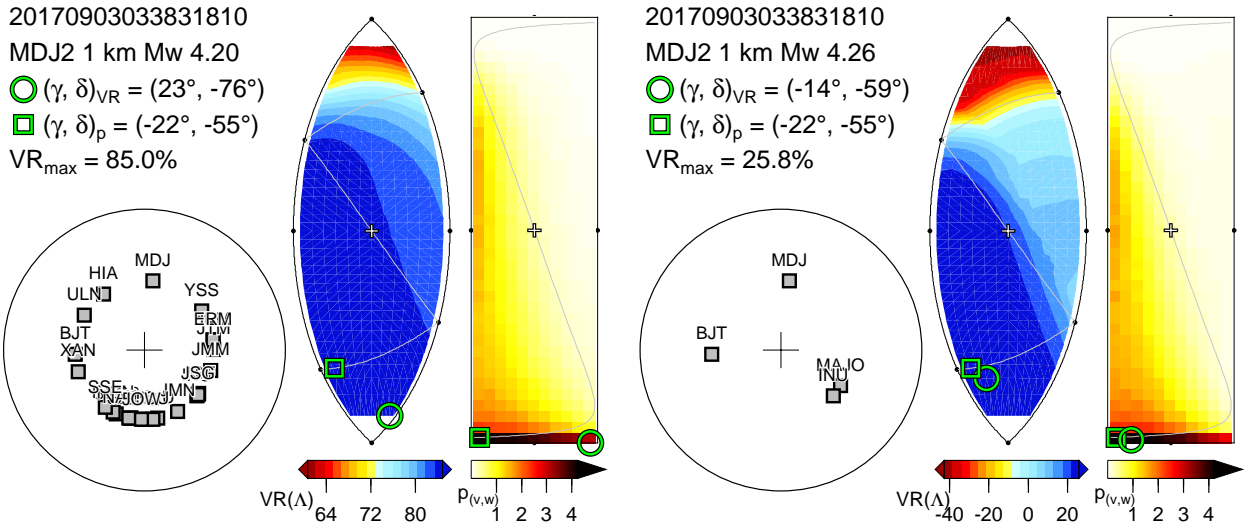


Figure D27: Moment tensor and uncertainties for NK6b using four stations (left) and all stations (right). The beachball is the best-fitting moment tensor, indicated by the white circle on the lune plot. The lune shows the variance reduction  $VR(\Lambda)$ . The  $vw$ -rectangle shows  $p(v, w)$ , the probability density for source type; the maximum of  $p(v, w)$  is denoted by the green circle.

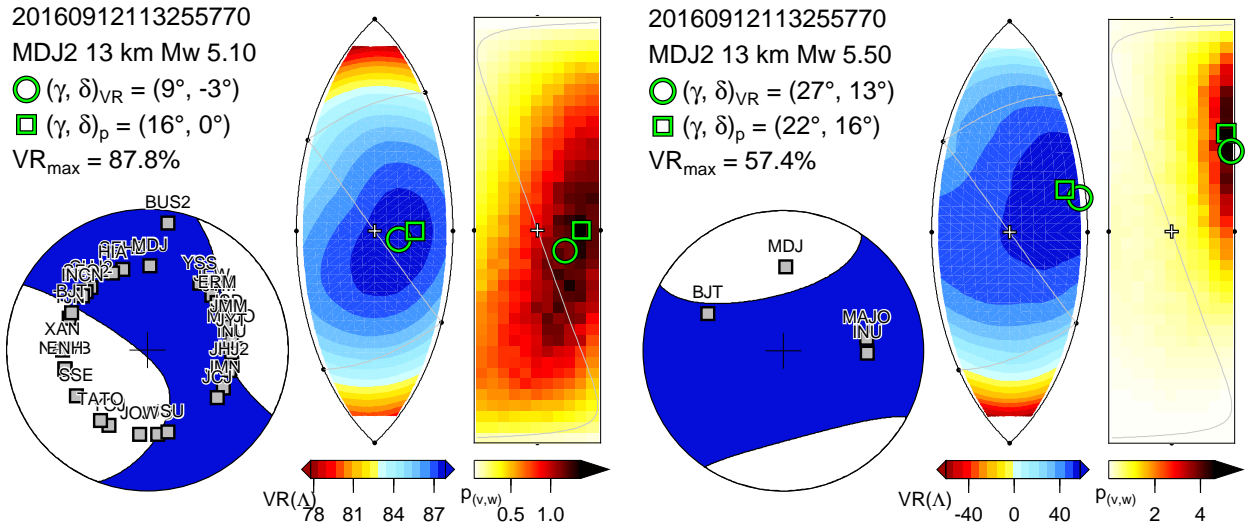


Figure D28: Moment tensor and uncertainties for EQ1 using four stations (left) and all stations (right). The beachball is the best-fitting moment tensor, indicated by the white circle on the lune plot. The lune shows the variance reduction  $VR(\Lambda)$ . The  $vw$ -rectangle shows  $p(v, w)$ , the probability density for source type; the maximum of  $p(v, w)$  is denoted by the green circle.

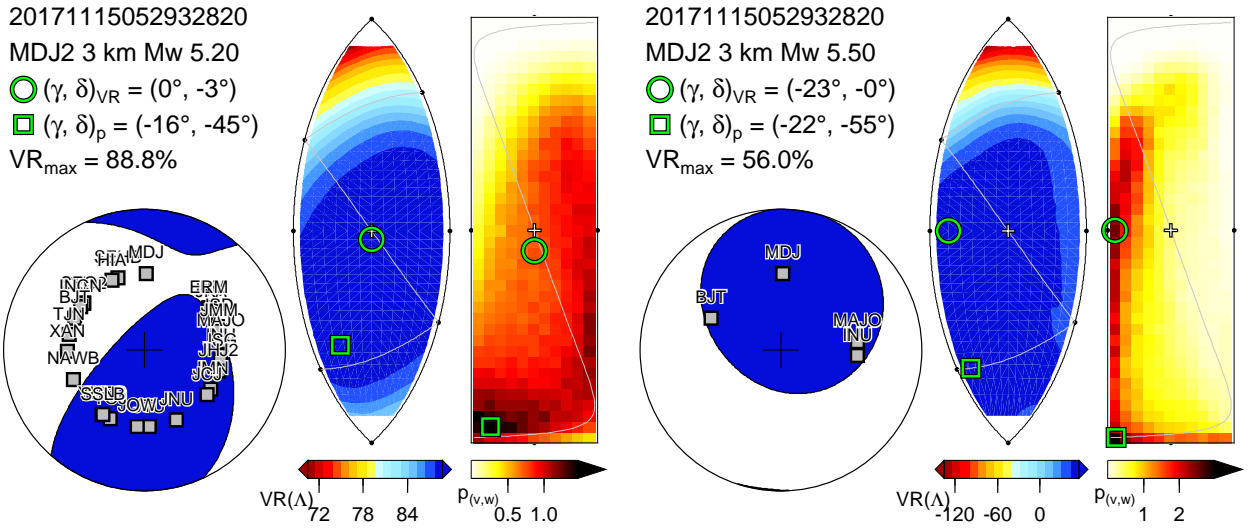


Figure D29: Moment tensor and uncertainties for EQ2 using four stations (left) and all stations (right). The beachball is the best-fitting moment tensor, indicated by the white circle on the lune plot. The lune shows the variance reduction  $VR(\Lambda)$ . The  $vw$ -rectangle shows  $p(v, w)$ , the probability density for source type; the maximum of  $p(v, w)$  is denoted by the green circle.